

Effects of photoionization on propagation and branching of positive and negative streamers in sprites

Ningyu Liu and Victor P. Pasko

Communications and Space Sciences Laboratory, Pennsylvania State University, University Park, Pennsylvania, USA

Received 27 May 2003; revised 27 December 2003; accepted 13 January 2004; published 3 April 2004.

[1] Modeling studies indicate that double-headed streamers originating from single electron avalanches in lightning-driven quasi-static electric fields at mesospheric altitudes accelerate and expand, reaching transverse scales from tens to a few hundreds of meters and propagation speeds up to one tenth of the speed of light, in good agreement with recent telescopic, high-speed video and multichannel photometric observations of sprites. The preionization of the medium ahead of a streamer by the ionizing UV photons originating from a region of high electric field in the streamer head (i.e., photoionization) significantly modifies the streamer scaling properties as a function of air pressure in comparison with those predicted by similarity laws. The photoionization leads to lower peak electric fields in the streamer head, lower streamer electron densities, wider initial streamer structures, and lower acceleration and expansion rates of streamers at sprite altitudes 40–90 km, when compared to the ground level. The primary reason for the observed differences is that the effective quenching altitude of the excited states of the molecular nitrogen $b^1\Pi_u$, $b'^1\Sigma_u^+$, and $c'_4{}^1\Sigma_u^+$ that give photoionizing radiation is about 24 km. The quenching of these states is therefore negligible at sprite altitudes, leading to a substantial enhancement of the electron-ion pair production ahead of the streamer tip because of the photoionization, when compared to the ground level. The maximum radius of the expanding streamers is predominantly controlled by the combination of the absorption cross section $\chi_{\min} = 3.5 \times 10^{-2} \text{ cm}^{-1} \text{ Torr}^{-1}$ of the molecular oxygen (O_2) at 1025 Å and the partial pressure of O_2 in air, p_{O_2} . Streamers exhibit branching when their radius becomes greater than $1/\chi_{\min} p_{\text{O}_2}$. Model results indicate a lower branching threshold radius for positive streamers in comparison with negative streamers, under otherwise identical ambient conditions. These results are in good agreement with recent results of high-speed photography of laboratory streamers in near-atmospheric pressure N_2/O_2 mixtures and similar morphology documented during recent telescopic and high-speed video observations of sprites. **INDEX TERMS:** 2427 Ionosphere: Ionosphere/atmosphere interactions (0335); 3304 Meteorology and Atmospheric Dynamics: Atmospheric electricity; 3324 Meteorology and Atmospheric Dynamics: Lightning; 0310 Atmospheric Composition and Structure: Airglow and aurora; 2435 Ionosphere: Ionospheric disturbances; **KEYWORDS:** corona streamers, photoionization, sprites

Citation: Liu, N., and V. P. Pasko (2004), Effects of photoionization on propagation and branching of positive and negative streamers in sprites, *J. Geophys. Res.*, 109, A04301, doi:10.1029/2003JA010064.

1. Introduction

[2] Sprites are large luminous discharges, which appear in the altitude range of ~ 40 to 90 km above large thunderstorms [e.g., Sentman *et al.*, 1995]. Recent telescopic imaging of sprites revealed an amazing variety of generally vertical fine structure with transverse spatial scales ranging from tens to a few hundreds of meters [Gerken *et al.*, 2000; Gerken and Inan, 2002, 2003]. Also recently, it has been demonstrated that sprites often exhibit a sharp altitude transition between the upper diffuse and the lower highly structured regions [Stenbaek-Nielsen *et al.*, 2000; Pasko and

Stenbaek-Nielsen, 2002; Gerken and Inan, 2002, 2003]. The appearance of the fine structure and vertical stratification in sprites has been interpreted in terms of positive and negative streamer coronas, which are considered as scaled analogs of small-scale streamers, which exist at high atmospheric pressures at ground level [e.g., Pasko *et al.*, 1998; Raizer *et al.*, 1998; Petrov and Petrova, 1999; Pasko *et al.*, 2001; Pasko and Stenbaek-Nielsen, 2002].

[3] Streamers are narrow filamentary plasmas, which are driven by highly nonlinear space charge waves [e.g., Raizer, 1991, p. 327]. The streamer polarity is defined by a sign of the charge in its head. The positive streamer propagates against the direction of the electron drift and requires ambient seed electrons avalanching toward the streamer head for the spatial advancement [e.g., Dhali and Williams,

1987]. The negative streamer is generally able to propagate without the seed electrons since electron avalanches originating from the streamer head propagate in the same direction as the streamer [e.g., *Vitello et al.*, 1994; *Rocco et al.*, 2002]. At low atmospheric pressures, at sprite altitudes, streamers may initiate from single electron avalanches in regions, where the electric field exceeds the conventional breakdown threshold field E_k defined by the equality of the ionization and dissociative attachment coefficients in air [e.g., *Raizer*, 1991, p. 135]. In this case double-headed streamers are expected to form [e.g., *Loeb and Meek*, 1940; *Kunhardt and Tzeng*, 1988; *Vitello et al.*, 1993] with the negative head propagating upward toward the ionosphere and the positive downward toward cloud tops (assuming the positive polarity of a typical cloud-to-ground lightning discharge producing sprites [e.g., *Hu et al.*, 2002]).

[4] The studies of streamers in air at ground pressure have been motivated for many years by their known ability to generate chemically active species, which can be used for treatment of hazardous and toxic pollutants [e.g., *Kulikovskiy*, 1997a; *van Veldhuizen*, 2002, and references cited therein]. It is well established by now that the dynamical properties and geometry of both positive and negative streamers can be affected by the population of the seed electrons, and many of the recent modeling studies have been devoted to understanding of the role of the ambient medium preionization, including effects of photoionization by UV photons originating from a region of high electric field in the streamer head, on the dynamics of negative [e.g., *Babaeva and Naidis*, 1997; *Rocco et al.*, 2002] and positive [e.g., *Babaeva and Naidis*, 1997; *Kulikovskiy*, 2000; *Pancheshnyi et al.*, 2001] streamers in different mixtures of molecular nitrogen (N_2) and oxygen (O_2) gases, and in air at ground pressure.

[5] The UV line intensities appearing in the spectra of terrestrial auroral and airglow observational data by rockets and high-altitude satellites contain important diagnostic information on energy input taking place into the thermosphere, and it is known from the related studies that the photoabsorption of N_2 and O_2 is significant below 240 km in the terrestrial atmosphere and that the highly structured ionization continuum of O_2 molecules appears below the ionization edge of 1027 Å, while the strong photoabsorption of N_2 starts below approximately 1000 Å [*Kanik et al.*, 2000]. As will be further discussed in section 2, in the narrow range 980–1025 Å the spectra of photoemission and photoabsorption of N_2 are not exactly the same and photons emitted by N_2 are not absorbed by N_2 and can lead to photoionization of O_2 . In air, the radiation in the wavelength range 980–1025 Å originates from the radiative transitions Birge-Hopfield I ($b_1\Pi_u \rightarrow X^1\Sigma_g^+$), Birge-Hopfield II ($b^1\Sigma_u^+ \rightarrow X^1\Sigma_g^+$) and Carroll-Yoshino Rydberg ($c^1\Sigma_u^+ \rightarrow X^1\Sigma_g^+$) of N_2 , which can be initiated by impact excitation of the $b^1\Pi_u$, $b^1\Sigma_u^+$ and $c^1\Sigma_u^+$ states of N_2 by energetic streamer electrons [e.g., *Zheleznyak et al.*, 1982]. We note that because of the relatively short absorption path at the sprite altitudes, it is not likely that the UV emissions responsible for photoionization in sprite streamers are directly observable from high-altitude satellites and rockets (see further discussion on photoionization range in section 4.4).

[6] The importance of the photoionization effects on sprite streamers at low air pressures at high altitudes is

underscored by the fact that the effective quenching altitude of the excited states $b^1\Pi_u$, $b^1\Sigma_u^+$ and $c^1\Sigma_u^+$ that give the photoionizing radiation is about 24 km (corresponding to the air pressure $p = p_q = 30$ Torr) [e.g., *Zheleznyak et al.*, 1982]. The quenching of these states is therefore negligible at typical sprite altitudes 40–90 km, leading to an enhancement of the electron-ion pair production ahead of the streamer tip because of the photoionization, when compared to the previous studies of streamers at ground level. These effects have not yet been accounted for in the existing models of sprite streamers [e.g., *Pasko et al.*, 1998; *Raizer et al.*, 1998]. The purpose of this paper is to evaluate a role of the photoionization effects on propagation properties of double-headed streamers initiated from single electron avalanches at low air pressures corresponding to sprite altitudes.

2. Model Formulation

[7] We describe the dynamics of streamers by a cylindrically symmetric numerical model similar to those employed in the recent studies of streamers at ground pressure [e.g., *Babaeva and Naidis*, 1997; *Kulikovskiy*, 2000, and references therein]. The model includes the electron and ion convection-diffusion equations coupled with the Poisson's equation:

$$\frac{\partial n_e}{\partial t} + \nabla \cdot n_e \vec{v}_e - D_e \nabla^2 n_e = (\nu_i - \nu_{a2} - \nu_{a3})n_e - \beta_{ep}n_en_p + S_{ph} \quad (1)$$

$$\frac{\partial n_p}{\partial t} = \nu_i n_e - \beta_{ep}n_en_p - \beta_{np}n_n n_p + S_{ph} \quad (2)$$

$$\frac{\partial n_n}{\partial t} = (\nu_{a2} + \nu_{a3})n_e - \beta_{np}n_n n_p \quad (3)$$

$$\nabla^2 \phi = -\frac{e}{\epsilon_0} (n_p - n_e - n_n) \quad (4)$$

where n_e , n_p , and n_n are the electron, positive ion, and negative ion number densities, \vec{v}_e is the drift velocity of electrons, ν_i is the ionization coefficient, ν_{a2} , and ν_{a3} are the two-body and three-body electron attachment coefficients, respectively, β_{ep} and β_{np} are the coefficients of electron positive ion and negative-positive ion recombination, respectively, D_e is the electron diffusion coefficient, S_{ph} is the rate of electron-ion pair production due to photoionization, ϕ is the electric potential, e is the absolute value of electron charge, and ϵ_0 is the permittivity of free space. The electron drift velocity is defined as $\vec{v}_e = -\mu_e \vec{E}$, where μ_e is the absolute value of the electron mobility and $\vec{E} = -\nabla \phi$ is the electric field. On timescales of interest for studies presented in this paper the ions are assumed to be motionless. This assumption is fully justified by the fact that mobilities of positive and negative ions are two orders of magnitude lower than the electron mobility [e.g., *Kulikovskiy*, 2000].

[8] The continuity equations (1), (2), and (3) effectively represent a fluid description of streamer plasma based on a first moment of the Boltzmann kinetic equation [e.g., *Guo and Wu*, 1993]. The coefficients of the model are assumed to be functions of the local reduced electric field E/N , where E is the electric field magnitude and N is the air neutral

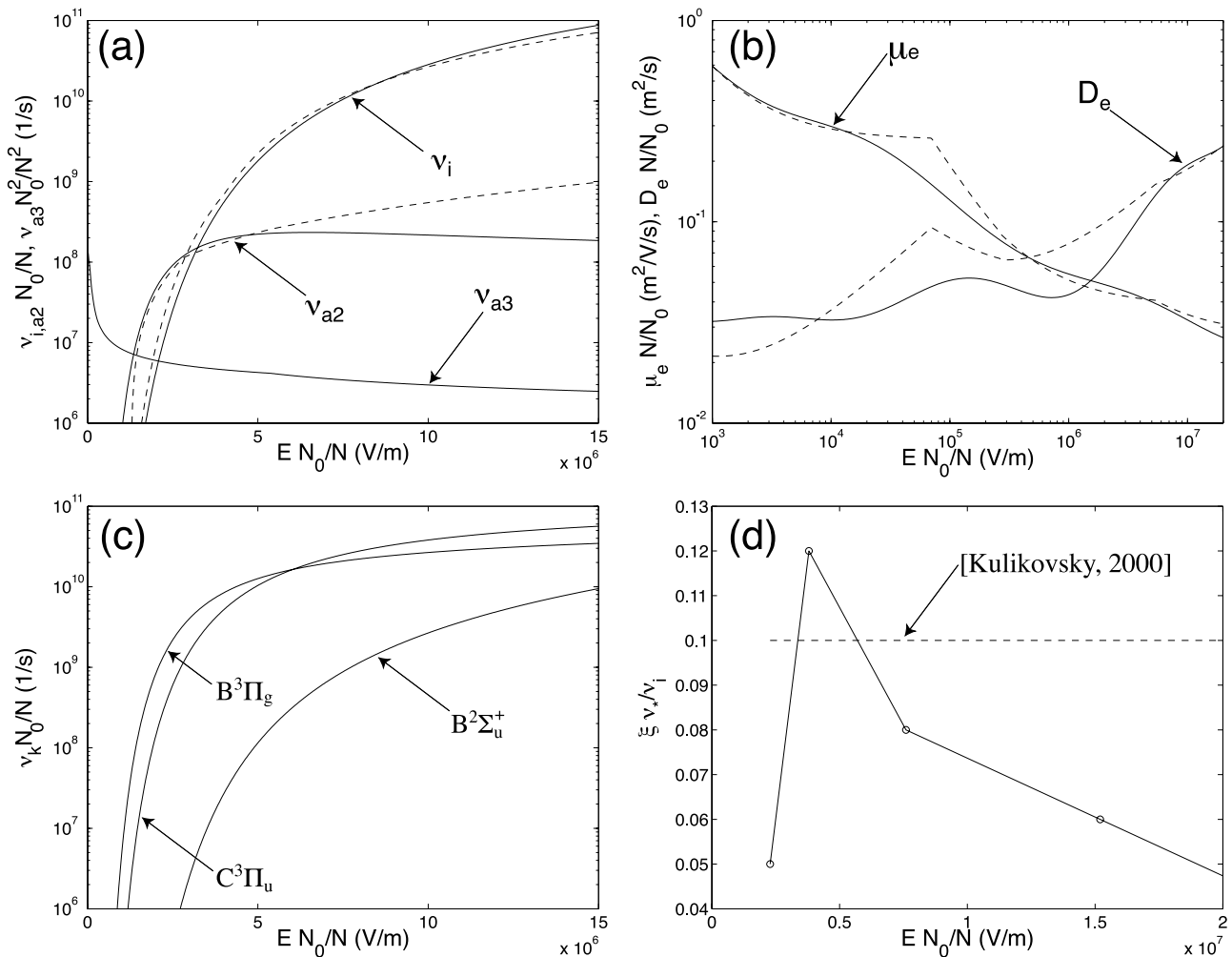


Figure 1. (a) The ionization ν_i , two-body ν_{a2} , and three-body ν_{a3} attachment coefficients, (b) the electron mobility μ_e and electron diffusion coefficient D_e , and (c) the optical excitation coefficients ν_k , are shown as a function of the reduced electric field in air, and (d) the quantity $\xi \nu_*/\nu_i$ (see text for details).

density. This implies that the equilibrium electron distribution function is achieved instantaneously in time in response to the applied local electric field E . This assumption is justified as soon as relaxation times of the mean energy and momentum of the electron distribution remain substantially less than the timescales characterizing variations of the electric field. In particular, at ground pressure the energy relaxation timescales are on the order of 10 ps, and 1 ps, for the typical electric field magnitudes in the streamer body, and streamer head, respectively [Vitello *et al.*, 1993; Guo and Wu, 1993]. The local field approximation is therefore justified on typical timescales of streamer development, which are usually measured in nanoseconds. We note that the variations of parameters of streamer plasma due to the large space and time derivatives of the reduced electric field and electron density near the streamer head, do introduce measurable corrections to the streamer dynamics [Naidis, 1997]. However, from the point of view of practical accuracy, the local approach provides a satisfactory representation of the streamer characteristics [Naidis, 1997]. The 1–10 ps, scaled ($\sim 1/N$) with atmospheric density, correspond to 0.07–0.7 ns, and 15–150 ns at altitudes 30 km, and 70 km, respectively. The validity of the local field

approximation therefore remains in force for sprite streamers developing on timescales of hundreds of ns, and tens of μs at altitudes 30 km, and 70 km, respectively (see modeling results presented in section 3 and discussion of streamer similarity laws in sections 3 and 4.2).

[9] The model ionization coefficient ν_i , two-body (dissociative) attachment coefficient ν_{a2} , the electron mobility μ_e and the electron diffusion coefficient D_e as functions of the reduced electric field in air are obtained from solutions of the Boltzmann equation [Pasko *et al.*, 1999; Barrington-Leigh, 2000; Barrington-Leigh *et al.*, 2002]. The model for the three-body attachment coefficient ν_{a3} is adopted from [Morrow and Lowke, 1997]. For fast model execution all coefficients as functions of the reduced electric field were represented in a form of lookup tables. The corresponding distributions used in our modeling are shown by solid lines in Figures 1a and 1b. Significant quantitative differences exist between different models and experimental measurements of ν_i , ν_{a2} , ν_{a3} , μ_e , and D_e in air available in the literature [e.g., Dutton, 1975; Gallagher *et al.*, 1983; Davies, 1983; Lowke, 1992; Morrow and Lowke, 1997, and references therein]. As illustration of the existing variability Figures 1a and 1b show by dashed lines model representa-

tions of ν_i , ν_{a2} , μ_e , and D_e provided by *Morrow and Lowke* [1997]. Although the distributions provided by *Morrow and Lowke* [1997] appear to be similar to those, which are used in our studies (see Figures 1a and 1b), calculations with our model, when repeated with parameters specified by *Morrow and Lowke* [1997], led to results, which exhibited numerical deviations of streamer characteristics (i.e., those summarized in Tables 2 and 3) as large as 20%. However, within the 20% variability all the features of streamer dynamics reported in this paper (i.e., streamer acceleration and expansion, quenching effects, etc.) remained essentially the same, and conclusions of this study therefore are not affected by the existing uncertainties in the model coefficients.

[10] Assuming that O_2^+ is the dominant positive ion in the streamer plasma [e.g., *Naidis*, 1999], the electron positive ion recombination coefficient is defined as $\beta_{ep} = 1.138 \times 10^{-11} T_e^{-0.7} \text{ m}^3/\text{s}$ [*Zhao et al.*, 1995], where T_e is the effective electron temperature in $^\circ\text{K}$ evaluated as $T_e = eD_e/\mu_e k_B$, where k_B is the Boltzmann's constant. The coefficient of the negative-positive ion recombination is defined as $\beta_{np} = 2 \times 10^{-13} (300/T)^{0.5} \text{ m}^3/\text{s}$ [*Kossyi et al.*, 1992], where T is the temperature of air, which is assumed to have a constant value of 300°K in all simulations presented in this paper. We note that on relatively short timescales considered in our studies presented in this paper (i.e., several ns at ground pressure) the effects of the attachment and recombination are small. These processes, however, are known to be important for the dynamics of long streamers developing in point-to-plane discharge gaps in low electric fields ($< E_k$) [e.g., *Morrow and Lowke*, 1997].

[11] For calculation of optical emissions we use a model similar to that documented by *Pasko et al.* [1997]. The intensity of each optical emission in Rayleighs is given by the expression [*Chamberlain*, 1978, p. 213]:

$$I_k = 10^{-6} \int_{L'} A_k n_k dl \quad (5)$$

where n_k [$1/\text{cm}^3$] is the number density of excited particles in state k , A_k [$1/\text{s}$] is the radiation transition rate, and the integral is taken along L' [cm], representing the horizontal line of sight. Our calculations in this paper, do not take into account the effects of radiative transfer between the source of the emission and the observer.

[12] The quantity n_k is governed by the relation [*Sipler and Biondi*, 1972]:

$$\frac{\partial n_k}{\partial t} = -\frac{n_k}{\tau_k} + \sum_m n_m A_m + \nu_k n_e \quad (6)$$

where $\tau_k = [A_k + \alpha_1 N_{N_2} + \alpha_2 N_{O_2}]^{-1}$ is the total lifetime of state k , α_1 and α_2 are the quenching rates due to collisions with N_2 and O_2 molecules, respectively, N_{N_2} and N_{O_2} are the number densities of N_2 and O_2 molecules respectively, and the sum over the terms $n_m A_m$ represents increases in n_k resulting from cascading from higher-energy states.

[13] In this paper we report results on optical emissions from the first ($B^3\Pi_g \rightarrow A^3\Sigma_u^+$) and second ($C^3\Pi_u \rightarrow B^3\Pi_g^+$) positive bands of N_2 and the first negative bands of N_2^+ ($B^2\Sigma_u^+ \rightarrow X^2\Sigma_g^+$), which have been documented in sprites [*Mende et al.*, 1995; *Hampton et al.*, 1996; *Armstrong et al.*,

1998, 2000; *Suszcynsky et al.*, 1998; *Morrill et al.*, 1998, 2002; *Takahashi et al.*, 2000; *Bucselo et al.*, 2003]. The optical emissions from the first and second positive bands of N_2 , and the first negative bands of N_2^+ have the transition rates $A_k = 1.7 \times 10^5$ 1/s, 2×10^7 1/s and 1.4×10^7 1/s, respectively [*Vallance Jones*, 1974, p. 119]. Quenching of the $B^3\Pi_g$ state of N_2 and $B^2\Sigma_u^+$ state of N_2^+ occurs primarily through collisions with N_2 , with $\alpha_1 = 10^{-11} \text{ cm}^3/\text{s}$ and $\alpha_1 = 4 \times 10^{-10} \text{ cm}^3/\text{s}$, respectively [*Vallance Jones*, 1974, p. 119]. Quenching of the $C^3\Pi_u$ state of N_2 occurs primarily through collisions with O_2 molecules with $\alpha_2 = 3 \times 10^{-10} \text{ cm}^3/\text{s}$ [*Vallance Jones*, 1974, p. 119]. We use updated optical excitation coefficients as a function of the reduced electric field in air [*Pasko et al.*, 1999; *Barrington-Leigh*, 2000; *Barrington-Leigh et al.*, 2002; *Pasko and George*, 2002], which are shown in Figure 1c. The model calculates the full time dynamics of optical emissions (without the steady state assumption). The optical emission equations (6) are solved using a first-order finite difference method.

[14] The model accounts for the effects of photoionization on the streamer dynamics using a physical model proposed by *Zheleznyak et al.* [1982]. In accordance with the high-resolution studies of photoionization processes in O_2 , the threshold wavelength of the radiation to ionize O_2 is 1025 \AA [*Dehmer and Chupka*, 1975]. However, the radiation with the wavelength shorter than 980 \AA is heavily absorbed by N_2 [*Carter*, 1972]. Thus, in the streamer process the photoionization of O_2 is caused by the radiation in the region of the spectrum $980 < \lambda < 1025 \text{ \AA}$ [*Zheleznyak et al.*, 1982]. The radiation in the interval $980 < \lambda < 1025 \text{ \AA}$ is produced because of the radiative transitions from three singlets of N_2 ($b^1\Pi_u$, $b^1\Sigma_u^+$ and $c^1\Sigma_u^+$) to the ground state ($X^1\Sigma_g^+$). These three radiative transitions are named as Birge-Hopfield I ($b^1\Pi_u \rightarrow X^1\Sigma_g^+$), Birge-Hopfield II ($b^1\Sigma_u^+ \rightarrow X^1\Sigma_g^+$), and Carroll-Yoshino Rydberg ($c^1\Sigma_u^+ \rightarrow X^1\Sigma_g^+$), respectively [e.g., *Kanik et al.*, 2000]. Though N_2 is the source of the radiation, the absorption of the radiation by N_2 molecules is negligible because of the asymmetry of the excitation and radiation mechanism of the singlet states of N_2 in streamers. The asymmetry is explained by *Zheleznyak et al.* [1982] as follows. In streamer discharges, which are usually associated with relatively low current densities, the temperature for populating vibrational levels of N_2 is not high and practically all molecules are located in the vibrational level $v'' = 0$ of the ground state $X^1\Sigma_g^+$. Collisions with electrons populate the vibrational levels v' of the radiating states $b^1\Pi_u$, $b^1\Sigma_u^+$ and $c^1\Sigma_u^+$, and the emission spectrum forms as a result of the radiative transitions $v' \rightarrow v''$. The concentration of molecules at levels $v'' \neq 0$ is low and absorption from them is insignificant. The ground level $X^1\Sigma_g^+$ ($v'' = 0$) begins to absorb radiation with the wavelength of 980 \AA , which corresponds to the energy difference between the lower vibrational levels of the ground and emitting state. Thus photons with $\lambda > 980 \text{ \AA}$, arising as a results of radiative transitions $v' \rightarrow v''$, are not absorbed by N_2 and can ionize O_2 .

[15] In the photoionization model, the number of ionization events dQ_{ph} in volume dV_2 per unit time owing to the absorption of photons emitted per unit time from superposition of elementary volumes dV_1 of the source at a distance $r = |\vec{r}_1 - \vec{r}_2|$, where \vec{r}_1 and \vec{r}_2 are radius vectors,

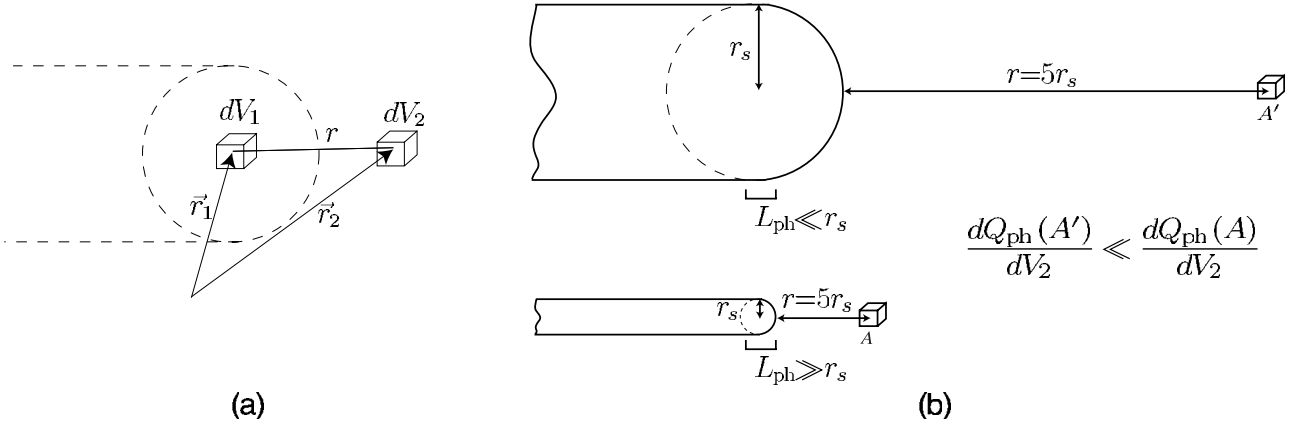


Figure 2. (a) Geometry of the photoionization model. (b) Schematics illustrating the principal length scales of the photoionization model.

determining the positions of elementary volumes dV_1 and dV_2 (Figure 2a), can be expressed in the form $dQ_{\text{ph}} = S_{\text{ph}}dV_2$, where

$$S_{\text{ph}} = \frac{dQ_{\text{ph}}}{dV_2} = \int_{V_1} \frac{\varphi(r)}{4\pi r^2} dV_1 \quad (7)$$

$$\varphi(r) = \int \varepsilon_f \xi_f k_f e^{-k_f r} df \quad (8)$$

and where ε_f is the emissivity of the gas ($\varepsilon_f df$ is the number of photons emitted per unit volume per unit time in the frequency interval $[f, f + df]$), k_f is the absorption coefficient, and ξ_f is the probability of ionization through absorption of a photon with a frequency of f [Zheleznyak *et al.*, 1982; Mnatsakanyan and Naidis, 1991]. The integral equation (8) can be approximated as a sum over frequency regions Δf characterized by different values of the absorption coefficient [Mnatsakanyan and Naidis, 1991]:

$$\varphi(r) = \sum_i \frac{\xi_i q_i}{\Delta f_i} \int_{\Delta f_i} k_f e^{-k_f r} df \quad (9)$$

where ξ_i is the average value of ξ_f in the interval Δf_i , and $q_i = \int_{\Delta f_i} \varepsilon_f df$. In the interval $980 < \lambda < 1025$ Å, the absorption coefficient of O_2 is a sharp function of frequency of the form [Mnatsakanyan and Naidis, 1991]:

$$k_f = k_1 (k_2/k_1)^{(f-f_1)/(f_2-f_1)} \quad (10)$$

where $k_1 = \chi_{\text{min}} p_{\text{O}_2}$, $k_2 = \chi_{\text{max}} p_{\text{O}_2}$, and $\chi_{\text{min}} = 0.035 \text{ Torr}^{-1} \text{ cm}^{-1}$ and $\chi_{\text{max}} = 2 \text{ Torr}^{-1} \text{ cm}^{-1}$ are, respectively, the minimum and maximum absorption cross sections of O_2 in the interval 980–1025 Å [Zheleznyak *et al.*, 1982]. The substitution of equation (10) into equation (9) and straightforward integration of equation (9) (here the spectral range 980–1025 Å is treated as a single frequency element range) leads to

$$\varphi(r) = \frac{\xi q}{r \ln(k_2/k_1)} (e^{-k_1 r} - e^{-k_2 r}) \quad (11)$$

where ξ is the average photoionization efficiency in the interval 980–1025 Å, and $q = \int_{\Delta f} \varepsilon_f df$ over the frequency range corresponding to 980–1025 Å. The quantity q can be expressed as [Zheleznyak *et al.*, 1982]:

$$q = \frac{p_q}{p + p_q} q_0 \quad (12)$$

where $p_q/(p + p_q)$ is a quenching multiplier (p is the gas pressure and p_q is the quenching pressure of the singlet states of N_2) and q_0 is the emissivity in the absence of quenching, which can be expressed in the form:

$$q_0 = \frac{\nu^*}{\nu_i} \nu_i n_e \quad (13)$$

where ν^* is the effective excitation coefficient for N_2 states transitions from which give the ionizing radiation, and ν_i and n_e are the previously introduced ionization coefficient and electron density, respectively. We note that in contrast to fully time-dependent model of optical emissions given by equation (6) the photoionization model of Zheleznyak *et al.* [1982] employs a steady state assumption, which in terms of equation (6) means that, without accounting for the cascading effects, at every moment of time $n_k/\tau_k = \nu_k n_e$, where, using the above introduced notations for the photoionizing emissions, $\nu_k \equiv \nu^*$, $\tau_k = \frac{1}{A_k} \frac{p_q}{p + p_q}$, and therefore $q = n_k A_k = \frac{p_q \nu^* n_e}{p + p_q}$ in agreement with equations (12) and (13). For the $b^1\Pi_u$, $b^1\Sigma_u^+$ and $c^4_1\Sigma_u^+$ states $A_k \approx 10^8 - 10^9 \text{ s}^{-1}$ [e.g., Walter *et al.*, 1994] and the steady state assumption is fully justified for streamers developing at air pressures corresponding to sprite altitudes. We note, however, that at high air pressures ($p \geq p_q$) the lifetime τ_k is comparable with timescales of variation of physical quantities in the streamer head (i.e., at ground pressure $\tau_k \approx 0.03 - 0.3 \text{ ns}$) and measurable deviations in streamer characteristics may result, when full time dynamics of these emissions is included in the model.

[16] Having substituted equation (13) into equation (12) and the resulting equation into equation (11), we obtain

$$\varphi(r) = \frac{p_q}{p + p_q} \xi \frac{\nu^*}{\nu_i} \nu_i n_e g(r) \quad (14)$$

Table 1. List of Reactions

Reaction Process	Reaction	Rate Coefficient and/or Reference
Ionization	$e + A \rightarrow 2e + A^+$	ν_i [s ⁻¹] (Figure 1a)
Photoionization	$h\nu + O_2 \rightarrow e + O_2^+$	S_{ph} [m ⁻³ s ⁻¹] (equations (7), (14), and (15))
Two-body attachment	$e + O_2 \rightarrow O^- + O$	ν_{a2} [s ⁻¹] (Figure 1a)
Three-body attachment	$e + O_2 + A \rightarrow O_2^- + A$	ν_{a3} [s ⁻¹] (Figure 1a)
Electron-ion recombination	$e + A^+ \rightarrow A$	$\beta_{ep} = 1.138 \times 10^{-11} T_e^{-0.7}$ [m ³ s ⁻¹] (see text)
Ion-ion recombination	$A^+ + B^- \rightarrow A + B$	$\beta_{np} = 2 \times 10^{-13} (300/T)^{0.5}$ [m ³ s ⁻¹] (see text)
Electron-impact excitation	$e + N_2 \rightarrow e + N_2(B^3\Pi_g)$	ν_k [s ⁻¹] (Figure 1c)
	$e + N_2 \rightarrow e + N_2(C^3\Pi_u)$	ν_k [s ⁻¹] (Figure 1c)
	$e + N_2 \rightarrow e + N_2^+(B^2\Sigma_u^+)$	ν_k [s ⁻¹] (Figure 1c)
	$e + N_2 \rightarrow e + N_2(b^1\Pi_u)$	ν_* [s ⁻¹] (equation (13))
	$e + N_2 \rightarrow e + N_2(b'^1\Sigma_u^+)$	ν_* [s ⁻¹] (equation (13))
	$e + N_2 \rightarrow e + N_2(c'_4^1\Sigma_u^+)$	ν_* [s ⁻¹] (equation (13))
Quenching	$N_2(B^3\Pi_g) + N_2 \rightarrow 2N_2$	$\alpha_1 = 10^{-11}$ [cm ³ s ⁻¹]
	$N_2(C^3\Pi_u) + O_2 \rightarrow N_2 + O_2$	$\alpha_2 = 3 \times 10^{-10}$ [cm ³ s ⁻¹]
	$N_2^+(B^2\Sigma_u^+) + N_2 \rightarrow N_2^+ + N_2$	$\alpha_1 = 4 \times 10^{-10}$ [cm ³ s ⁻¹]
	$N_2(b^1\Pi_u) + A \rightarrow N_2 + A$	$p_q = 30$ Torr
	$N_2(b'^1\Sigma_u^+) + A \rightarrow N_2 + A$	$p_q = 30$ Torr
	$N_2(c'_4^1\Sigma_u^+) + A \rightarrow N_2 + A$	$p_q = 30$ Torr
Optical emission		
First positive bands of N ₂	$N_2(B^3\Pi_g) \rightarrow N_2(A^3\Sigma_u^+) + h\nu$	$A_k = 1.7 \times 10^5$ [s ⁻¹]
Second positive bands of N ₂	$N_2(C^3\Pi_u) \rightarrow N_2(B^3\Pi_g) + h\nu$	$A_k = 2.0 \times 10^7$ [s ⁻¹]
First negative bands of N ₂ ⁺	$N_2^+(B^2\Sigma_u^+) \rightarrow N_2^+(X^2\Sigma_g^+) + h\nu$	$A_k = 1.4 \times 10^7$ [s ⁻¹]
Photoionizing emission		
Birge-Hopfield I	$N_2(b^1\Pi_u) \rightarrow N_2(X^1\Sigma_g^+) + h\nu$	equation (12)
Birge-Hopfield II	$N_2(b'^1\Sigma_u^+) \rightarrow N_2(X^1\Sigma_g^+) + h\nu$	equation (12)
Carroll-Yoshino Rydberg	$N_2(c'_4^1\Sigma_u^+) \rightarrow N_2(X^1\Sigma_g^+) + h\nu$	equation (12)

where

$$g(r) = \frac{\exp(-\chi_{\min} p_{O_2} r) - \exp(-\chi_{\max} p_{O_2} r)}{r \ln(\chi_{\max}/\chi_{\min})} \quad (15)$$

and k_1 and k_2 have been replaced in accordance with previously introduced notations by $\chi_{\min} p_{O_2}$ and $\chi_{\max} p_{O_2}$, respectively. The multiplier $\xi \nu_*/\nu_i$ appearing in equation (14) is provided in a table form as a function of the reduced electric field in [Zheleznyak *et al.*, 1982; Mnatsakanyan and Naidis, 1991, and references therein] and the corresponding distribution is reproduced in Figure 1d. A linear interpolation is used to find $\xi \nu_*/\nu_i$ for field values not specified in the table (i.e., between points shown by open circles in Figure 1d). We note that the model of Zheleznyak *et al.* [1982] specified by equations (7), (14), and (15) conveniently provides the photoelectron production rate in terms of the ionization rate $\nu_i n_e$. The reaction processes included in the model are summarized in Table 1.

[17] For the purposes of clarity, we would like to point out that in the description of the photoionization model given by Kulikovskiy [2000] the $C^3\Pi_u$ state of N₂ is incorrectly listed as a source of UV radiation leading to photoionization in air. The spectral range of the radiative transition from $C^3\Pi_u$ to the ground state $X^1\Sigma_g^+$ is from 1070 to 1130 Å [Lofthus and Krupenie, 1977]. The wavelength of radiation in this range is longer than the wavelength corresponding to the ionization threshold of O₂ [1025 Å] and therefore the radiation arising from $C^3\Pi_u$ state cannot ionize O₂ molecules. The model of Kulikovskiy [2000] expresses the photoelectron production rate in terms of the ionization rate assuming $\xi \nu_*/\nu_i = 0.1$, which is a reasonable approximation (see Figure 1d). The $C^3\Pi_u$ state therefore is not explicitly used in the modeling and does not affect correctness of results presented by Kulikovskiy [2000].

[18] We employ a modified Scharfetter-Gummel algorithm [Kulikovskiy, 1995] for solution of the electron convection-diffusion equation (1). The original Scharfetter-Gummel scheme [Scharfetter and Gummel, 1969] is widely used in studies of semiconductor and gas discharge plasma to solve the convection-dominated problems. It has a very important property of monotonicity, however, may result in highly diffused solutions, when the spatial resolution of the simulation is low. Kulikovskiy [1995] proposed a modified version of the original Scharfetter-Gummel scheme, which is based on introduction of virtual grid nodes and employment of exponential functions to represent sharp variations of the electron density, allowing to obtain a more accurate and less diffusive solution. Kulikovskiy [1995] simulated a one-dimensional shock wave propagation problem using three different algorithms: original Scharfetter-Gummel, modified Scharfetter-Gummel and flux-corrected transport (FCT) scheme [e.g., Zalesak, 1979]. When a high spatial resolution is used, the modified Scharfetter-Gummel and FCT schemes give almost identical results, which are very close to the exact solution. In contrast, the original Scharfetter-Gummel scheme leads to a very diffusive solution, which departs from the exact one by several orders of magnitude. When low resolution is used, FCT tends to produce a “staircase” on the wave curve, while modified Scharfetter-Gummel preserves the monotonicity [Kulikovskiy, 1995].

[19] The Poisson’s equation (4) is solved using the successive overrelaxation method (SSOR) [e.g., Hockney and Eastwood, 1988, p. 179] with modified boundary potential conditions to represent free dynamics of sprite streamers without effects of the electrode image charges [Babaeva and Naidis, 1996]. Figure 3 schematically shows the simulation domain used in our model. Two remote electrodes with a certain potential difference establish a

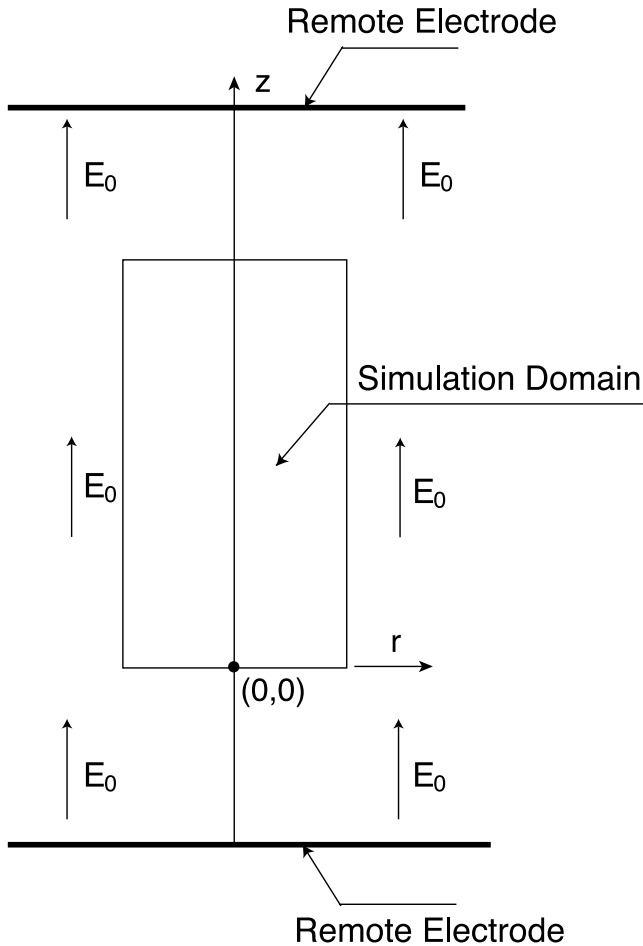


Figure 3. A cross-sectional view of the simulation domain.

homogeneous Laplacian field E_0 and streamers develop in the cylindrically symmetric simulation domain under influence of this applied field. Thus the total electric field has two components. One is the Laplacian field, and the another is the electric field generated by the space charges in the simulation domain. The solution for the electric potential can be represented in the following form [Babaeva and Naidis, 1996]:

$$\phi(\vec{r}) = \phi_L + \frac{1}{4\pi\epsilon_0} \iiint_{V'} \frac{\rho(\vec{r}')}{|\vec{r} - \vec{r}'|} dV' \quad (16)$$

where ϕ_L corresponds to the ambient Laplacian field, $\rho(\vec{r}')$ is the space charge density, \vec{r}' is the source point, \vec{r} is the observation point and the integral is taken over the volume containing space charges. The solution (16) is used to calculate the electric potential only at the boundary of the simulation domain. Inside the domain, the values of ϕ are computed by the SSOR method. By using this technique, a small simulation domain is sufficient to obtain an accurate solution for the electric potential corresponding to free (i.e., not affected by boundaries) dynamics of streamers.

[20] For the case studies presented in this paper we assume the applied electric field to be homogeneous with magnitudes $E_0 = 1.1E_k$, $1.25E_k$ and $1.5E_k$. At a typical sprite altitude of 70 km the chosen field magnitudes correspond to the light-

ning charge moment changes of 1800 C km, 2040 C km and 2450 C km, respectively [see Pasko *et al.*, 2001, Figure 1], which are well in the range of the measured charge moments required for sprite initiation, 120–3070 C km [Hu *et al.*, 2002]. We report results on dynamics of streamers at air pressures 760 Torr ($E_k \simeq 3.2 \times 10^6$ V/m), 11 Torr ($E_k \simeq 4.6 \times 10^4$ V/m) and 5×10^{-2} Torr ($E_k \simeq 220$ V/m), corresponding to altitudes 0, 30, and 70 km, respectively.

[21] For model runs presented in this paper we assume that the photoionization completely determines levels of preionization ahead of the streamers, and do not account for the ambient lower ionospheric electron population. The results reported here therefore are not applicable to the streamer-to-diffuse glow transition region of sprites [Pasko *et al.*, 1998; Pasko and Stenbaek-Nielsen, 2002], where this assumption becomes invalid.

3. Results

[22] Figure 4 shows results of model calculations of electron densities corresponding to double-headed streamers developing at altitudes 0, 30 and 70 km in electric field $E_0 = 1.5E_k$. For the purpose of improving computation efficiency, instead of the single electron initiation, the streamers were launched by placing clouds of plasma with peak densities 10^{14} , 2×10^{10} , and 5×10^5 cm $^{-3}$ and spherically symmetric Gaussian spatial distributions with characteristic scales 0.2 mm, 1.4 cm and 3 m, in the middle of the simulation domain at altitudes 0, 30, and 70 km, respectively. Test simulations of streamers initiated by single electron avalanches have also been conducted (not shown),

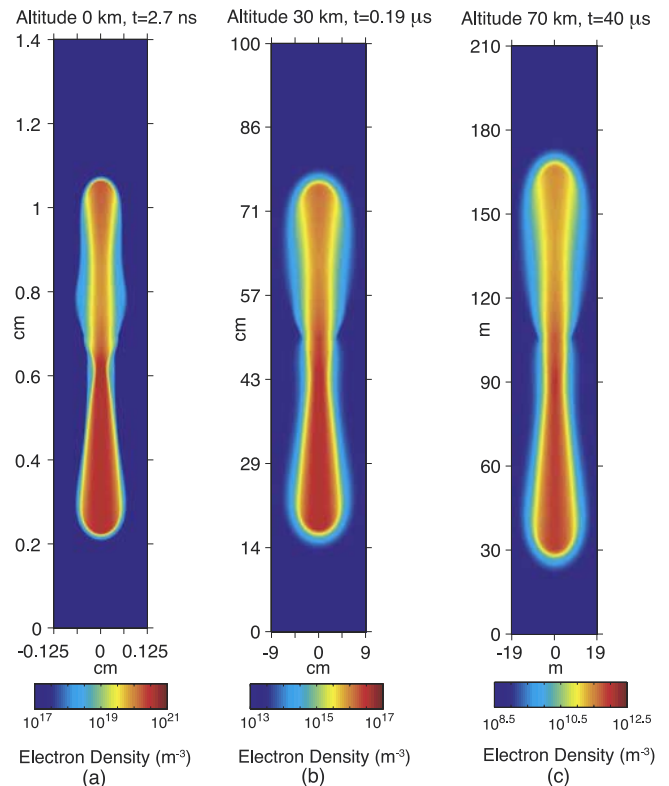


Figure 4. A cross-sectional view of the distribution of the electron number density of the model streamers at altitudes (a) 0, (b) 30, and (c) 70 km.

Table 2. Streamer Characteristics Measured at the Moments of Time Specified in Figure 4

Altitude, km	Streamer	E_h/E_k	E_b/E_k	N_s, m^{-3}	N_{oe}, m^{-3}	r_s, m	$v_s, \text{m s}^{-1}$	$v_d(E_h), \text{m s}^{-1}$	$\Delta U_h, V$	dr_s/dL	$dv_s/dL, \text{s}^{-1}$
0	Positive	6.7	0.44	3.16×10^{20}	7.94×10^{16}	4.0×10^{-4}	4.88×10^6	5.70×10^5	8920	0.0747	8.77×10^8
0	Negative	5.5	0.86	1.58×10^{20}	2.51×10^{16}	3.0×10^{-4}	2.96×10^6	4.90×10^5	-5780	0.0457	8.31×10^8
30	Positive	4.8	0.68	3.16×10^{16}	7.94×10^{13}	0.029	3.99×10^6	4.47×10^5	6950	0.0704	9.58×10^6
30	Negative	3.7	0.99	1.26×10^{16}	6.30×10^{13}	0.029	2.42×10^6	3.66×10^5	-4820	0.0494	8.36×10^6
70	Positive	4.6	0.73	7.08×10^{11}	5.01×10^9	6.5	4.88×10^6	4.34×10^5	7408	0.067	5.29×10^4
70	Negative	3.5	0.99	2.45×10^{11}	3.16×10^9	6.8	2.68×10^6	3.60×10^5	-5361	0.0565	4.20×10^4

and the results indicate that the streamers initiated by the clouds of relatively dense plasma attain similar characteristics to those initiated by single electron avalanches with a factor of ~ 10 reduction in the model execution time. Our modeling approach to initiation of streamers is supported by previous findings of Vitello *et al.* [1993], indicating that the introduction of a relatively dense plasma with densities and spatial scales of the same order of magnitude as expected in streamers, which develop from these perturbations, allows to effectively bypass the initial avalanche phase of the streamer development.

[23] In accordance with the similarity laws, the streamer timescales, the streamer spatial scales, and the streamer electron density scale with the air density as $\sim N$, $\sim 1/N$, and $\sim N^2$, respectively, and the scaled streamer characteristics remain otherwise identical for the same values of the reduced electric field E/N [Pasko *et al.*, 1998].

[24] In order to facilitate discussion of similarity properties of streamers at different altitudes/air densities, the results presented in Figures 4b and 4c are given at the moments of time, which are obtained by scaling ($\sim 1/N$) of the ground value, 2.7 ns, specified in Figure 4a. The horizontal and vertical dimensions of the simulation boxes in Figures 4b and 4c also directly correspond to scaled ($\sim N$) ground values shown in Figure 4a. The electron density scale in Figures 4b and 4c also corresponds to scaled ($\sim N^2$) values given in Figure 4a. Simple visual inspection of Figure 4 indicates a nearly similar behavior of streamers corresponding to 30 and 70 km altitudes, but the positive and negative streamer heads at ground pressure exhibit radial scales, respectively, $\sim 10\%$ and $\sim 50\%$ narrower than the corresponding scaled values at higher altitudes. Hereafter we define a streamer head radius r_s as a radial point at which the electron density is $1/e$ of its axis value. We note that the three-body electron attachment and electron positive ion recombination processes may lead to nonsimilar behavior of streamers at high gas pressures [e.g., Babaeva and Naidis, 2001]. However, simple estimates using ν_{a3} and β_{ep} coefficients specified in section 2 indicate that on timescales of simulations presented in Figure 4 these processes do not significantly affect the streamer properties. The photoionization model of [Zheleznyak *et al.*, 1982] is fully similar at typical sprite altitudes ~ 40 – 90 km. However, the similarity is not preserved at lower altitudes because of the quenching effects discussed in the introduction section. Our assertion therefore is that the differences observed between streamers at the ground and at 30 and 70 km altitudes in Figure 4 are primarily due to the reduction in photoelectron production at high atmospheric pressures through the quenching of UV emitting excited states of N_2 . This effect will be further discussed in the discussion section.

[25] Table 2 provides summary of streamer characteristics measured at the moments of time specified in Figure 4.

These characteristics include the peak electric field in the streamer head (E_h), the field in the streamer body (E_b), the streamer electron density (N_s), the electron density ahead of the streamer at a distance of one streamer radius from the streamer front (N_{oe}), the streamer radius (r_s), the streamer velocity (v_s), the electron drift velocity in the peak electric field in the streamer head ($v_d(E_h)$), and the potential of the streamer head with respect to the ambient field potential (ΔU_h). The definitions of E_h , E_b , N_s , N_{oe} , and ΔU_h are illustrated in Figures 5a, 5b, and 5c, which provide axis profiles of the related streamer characteristics at selected instants of time corresponding to 70 km streamer shown in Figure 4c. In all cases considered the streamers exhibit exponential increase of r_s and v_s with time. At the same time in all the cases considered the increase of the r_s and v_s as a function of the streamer length L can very accurately be approximated by a linear function and the related slope characteristics dr_s/dL and dv_s/dL are provided in Table 2. Since both r_s and v_s are proportional to L , they themselves have a linear relationship and the corresponding slope characteristic can be obtained by calculating the ratio $(dr_s/dL)/(dv_s/dL)$ using the data specified in Table 2. Our results indicate that positive streamers initially exhibit higher E_h/E_b ratios, electron densities and propagation velocities when compared with the negative ones (e.g., Figures 5a and 5b). These results qualitatively agree with properties of positive and negative streamers documented previously by other authors [Dhali and Williams, 1987; Vitello *et al.*, 1994; Babaeva and Naidis, 1997]. The observed streamer acceleration and expansion are also known features of streamers, which develop in relatively high applied electric fields. In this case the electric field in the streamer body, which is always lower than the ambient applied field, leads to a linear increase of the potential drop in the streamer head as a function of the streamer length, resulting in expansion of the streamer in order to maintain a quasi-constant E_h value [Babaeva and Naidis, 1997; Kulikovskiy, 1997b].

[26] We note that positive streamers in our simulations quickly reach a state of propagation with nearly constant E_h , E_b , N_s and N_{oe} values (shown in Table 2 and illustrated in Figures 5a and 5b), which do not change significantly on time and spatial scales of calculations presented in Figure 4. At the same time, by the end of simulations presented in Figure 4 the negative streamers have not yet reached a stable state of propagation, similar to positive streamers, and continue to exhibit increase in N_s and E_h and decrease in N_{oe} and E_b values (see Figures 5a and 5b). Therefore the data specified in Table 2 for negative streamers only accurately reflect their states at the time instants specified in Figure 4. Additional simulations (not shown) performed with long negative streamers indicate that the negative streamers always preserve with very high accuracy the expansion (dr_s/dL) and acceleration (dv_s/dL) characteristics specified

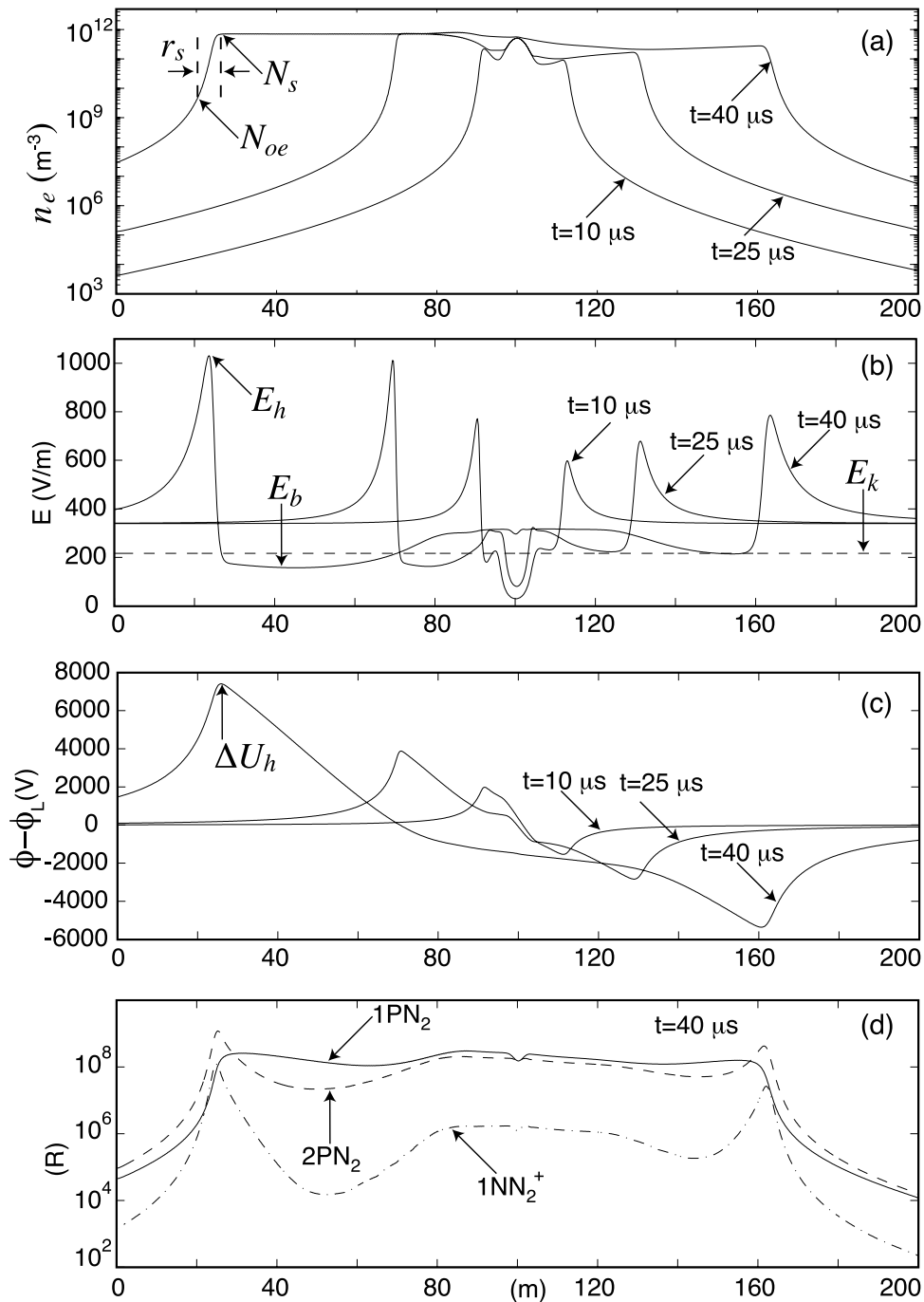


Figure 5. The profiles of streamer characteristics along the axis at selected instants of time corresponding to the model streamer shown in Figure 4c. (a) The electron density. (b) The electric field. (c) The relative electric potential $\phi - \phi_L$. (d) The intensity of optical emissions (in Rayleighs).

in Table 2, and as they grow longer accelerating and expanding, they tend to approach E_h , E_b , N_s and N_{oe} values similar to those of the positive streamers. This behavior is expected from simple analytical theory (see section 4.1) indicating diminishing of differences between positive and negative streamer heads, when $v_s \gg v_d(E_h)$.

[27] Table 3 gives examples illustrating changes in streamer characteristics with variation of the applied electric field. For the sake of brevity only data for positive streamers at 70 km altitude are shown at the time instants (the second

column) when streamers reached approximately the same length as in Figure 4c. The reduction of the applied electric field leads to a slower development of the streamers in time and a reduction in values of E_h , E_b , N_s , N_{oe} , r_s , v_s , $v_d(E_h)$, ΔU_h , dr_s/dL and dv_s/dL . We note that most of the streamer properties vary by only several tens of percent, generally remaining very similar at different applied electric fields. The only exception to this rule is v_s and dv_s/dL , which increase by $\sim 250\%$ in response to the electric field change from $1.1E_k$ to $1.5E_k$.

Table 3. Streamer Characteristics at Different Applied Electric Fields

E_0/E_k	Time, s	E_h/E_k	E_p/E_k	N_{s1}, m^{-3}	N_{oe2}, m^{-3}	r_{s1}, m	$v_{s1}, \text{m s}^{-1}$	$v_d(E_h), \text{m s}^{-1}$	$\Delta U_h, \text{V}$	dr_s/dL	$dv_s/dL, \text{s}^{-1}$
1.1	9.5×10^{-5}	4	0.51	3.98×10^{11}	3.16×10^9	5.2	2.04×10^6	3.98×10^5	5630	0.0506	1.94×10^4
1.25	7.0×10^{-5}	4.32	0.59	5.01×10^{11}	3.98×10^9	6.2	2.95×10^6	4.10×10^5	6830	0.0540	2.68×10^4
1.5	4.0×10^{-5}	4.6	0.73	7.08×10^{11}	5.01×10^9	6.5	4.88×10^6	4.34×10^5	7408	0.067	5.29×10^4

[28] Results of our model confirm a linear relationship between the potential growth in the streamer head relative to the ambient field potential distribution and the streamer radius [e.g., Raizer and Simakov, 1998, and references therein]. The related results presented in Tables 1 and 2 can be approximated by a simple relationship, $E_h = \gamma \Delta U_h / r_s$, where γ stays in the narrow range 0.8–1 for the cases considered.

[29] Figures 6 and 7 illustrate distributions of the electric field magnitude and intensities of optical emissions (in Rayleighs) corresponding to the model streamers at 30 and 70 km altitudes, respectively, at the same instants of time as specified in Figure 4. Figure 5d illustrates profiles along the axis of optical emission intensities corresponding to Figure 7. The spatial distributions of different optical emissions presented in Figures 6 and 7 can be readily interpreted in terms of the radiation transition rates, quenching properties and the excitation thresholds of the corresponding electronic states of the molecular nitrogen. The first positive bands of N_2 (1PN_2) have the lowest excitation threshold (~ 7.35 eV) and are effectively excited by electrons in the streamer head as well as in the relatively low fields in the streamer body (see Figures 6b and 7b). The effective lifetime of the 1PN_2 producing $B^3\Pi_g$ state is $3 \times$

10^{-7} s at 30 km altitude and 5.4×10^{-6} s at 70 km. At 30 km the lifetime is comparable to the overall time of the streamer formation and leads to the observed spreading of the optical emissions along the streamer body. This explains, in particular, why one does not observe the enhancement of 1PN_2 optical emissions due to the field enhancement around the tips of the streamers, which is apparent for both the 1st negative N_2^+ (1NN_2^+) and 2nd positive N_2 (2PN_2) bands, and underscores the importance to carry out the full time-dependent solution for optical emissions in the modeling of the streamer processes. The effective lifetime of the 2PN_2 producing $C^3\Pi_u$ state is 2.3×10^{-8} s at 30 km and 5×10^{-8} s at 70 km. At both altitudes, the lifetime is much less than the effective streamer formation time resulting in the observed enhancement of the 2PN_2 emission around the heads of the streamers. In this case the excited molecules emit photons almost instantaneously, when compared to the streamer formation and the overall model execution times, and the electric field enhancement around the streamer tip maps directly to the enhanced optical emissions in the same region of space. The 2PN_2 excitation threshold is ~ 11 eV and these emissions are also excited by the relatively low fields in the streamer body (see Figures 6c and 7c). The lifetime of the 1NN_2^+ producing $B^2\Sigma_u^+$ state is very short at both 30 km (7.5

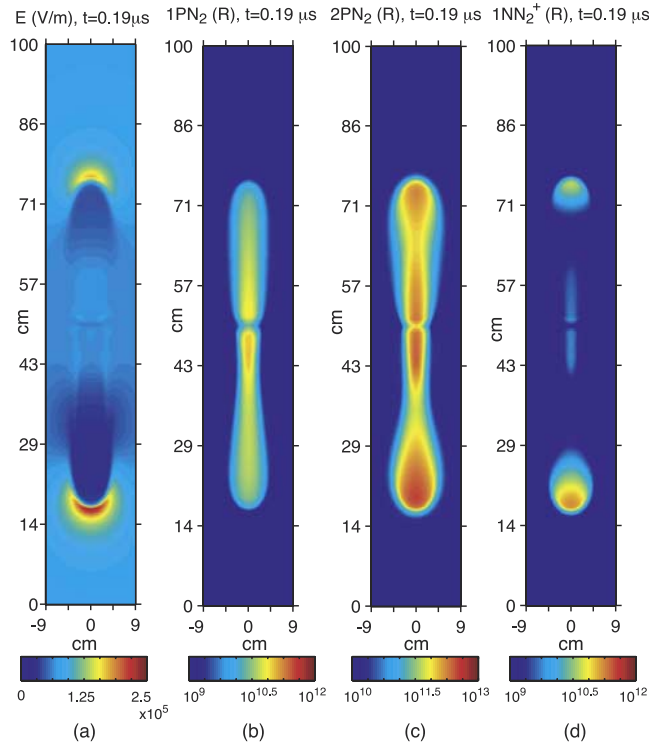


Figure 6. (a) The magnitude of the electric field and (b)–(d) the intensity of optical emissions in selected bands associated with the model streamers at altitude 30 km.

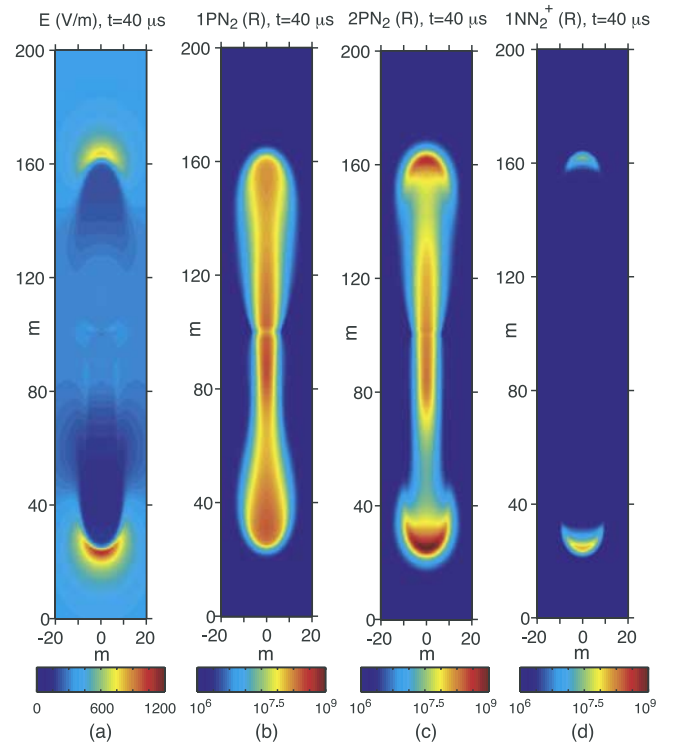


Figure 7. The same as Figure 6 only for model streamers at altitude 70 km.

$\times 10^{-9}$ s) and 70 km (6.9×10^{-8} s) altitudes. The $B^2\Sigma_u^+$ state also has the highest energy excitation threshold (~ 18.8 eV) among the optical emissions considered, and therefore the resultant $1NN_2^+$ emissions are mostly confined to the high field regions around streamer tips, as evident in Figures 5d, 6d, and 7d.

[30] The strong blue emissions ($1NN_2^+$ and $2PN_2$; Figures 7c and 7d) originating primarily in the streamer heads are expected to be produced during the early time of sprite development, as the sprite develops over its altitude extent on a timescale short with respect to the total sprite emission time. This agrees well with recent narrow band photometric and blue light video observations of sprites [Armstrong *et al.*, 1998, 2000; Suszcynsky *et al.*, 1998; Morrill *et al.*, 2002] indicating short duration (\sim ms) bursts of blue optical emissions appearing at the initial stage of sprite formation. The time averaged optical emissions are expected to be dominated by red emissions associated with the first positive bands of N_2 (Figures 5d and 7b), which have the lowest energy excitation threshold and can effectively be produced by relatively low electric fields in the streamer channels, in agreement with sprite observations [Mende *et al.*, 1995; Hampton *et al.*, 1996; Morrill *et al.*, 1998, 2002; Takahashi *et al.*, 2000; Bucseila *et al.*, 2003]. We note also, that the suppression of $1PN_2$ emissions due to the strong quenching of the $B^3\Pi_g$ state at altitudes below 50 km [e.g., Vallance Jones, 1974, p. 119] (note the intensity-scale difference between Figures 6b and 6c) is the primary factor which is responsible for making the blue color a dominant color of streamer coronas at lower extremities of sprites [e.g., Sentman *et al.*, 1995] and in blue jet type phenomena observed near thundercloud tops [e.g., Wescott *et al.*, 1995]. The red ($1PN_2$) emissions are not completely quenched at altitudes < 50 km and have been detected in red filtered images of sprites [Armstrong *et al.*, 1998]. A detailed calculation of the streamer color requires knowledge of the spectral range of the color TV system, the specifics of the observational geometry, allowing to account for the effects of the atmospheric transmission, and such factors as the transmission through an aircraft window [e.g., Wescott *et al.*, 1998; Morrill *et al.*, 1998]. These calculations are beyond the scope of the present paper. The interested readers can find more discussion on related topics in section 4.2 of Pasko and George [2002, and references therein].

4. Discussion

4.1. Effects of Preionization on Streamers

[31] The quenching multiplier $p_q/(p + p_q)$ appearing in [Zheleznyak *et al.*, 1982] photoionization model given by equations (7), (14), and (15), which leads to nonsimilar behavior of streamers at high pressures, is equal to $1/28.5$, $1/1.39$, and 1 at altitudes of 0, 30 and 70 km, respectively. At altitudes 30 and 70 km considered in Figure 4 the photoionization rate is therefore enhanced with respect to the ground level by factors 20.5 and 28.5, respectively. The streamers preserve similarity at high altitudes, where quenching effects are negligible (i.e., $p \ll p_q$ and $p_q/(p + p_q) \simeq 1$), which is a valid assumption for a typical altitude range of sprites 40–90 km. The enhancement of the electron density ahead of the streamer at high altitudes because of the enhanced photoionization represents the primary reason for the

observed differences in streamer properties presented in Figure 4 and Table 2. Indeed, for the positive streamer at the ground level from Table 2 we obtain $N_s/N_{oe} = 4000$, while at 70 km $N_s/N_{oe} = 141$. The ratio of the two is almost exactly the quenching factor between these altitudes discussed above (i.e., 28.5). As a result of the enhancement of the electron density ahead of the streamer at 70 km the ratio $E_h/E_b = 6.3$ is substantially lower than $E_h/E_b = 15.2$ observed at the ground level (see Table 2). The ground value of $N_s = 3.16 \times 10^{20} \text{ m}^{-3}$, when scaled to 70 km altitude ($\sim N^2$) becomes $1.45 \times 10^{12} \text{ m}^{-3}$, which is a factor of two greater than observed in our calculations $N_s = 7.08 \times 10^{11} \text{ m}^{-3}$. The enhancement of preionization therefore leads to the reduction in N_s and E_h/E_b in addition to the widening of the streamer radius (as already discussed in section 3). We emphasize, that although initially streamers at the ground level appear to be narrower than those at 30 and 70 km altitudes (Figure 4), the rate of the streamer expansion (dr_s/dL) and the scaled ($\sim N$) rate of streamer acceleration (dv_s/dL) exceed those corresponding to 30 and 70 km altitudes (Table 2) and long streamers at the ground pressure are expected to move faster and have wider effective radial scales, when compared to scaled streamers at sprite altitudes.

[32] Pancheshnyi *et al.* [2001] have recently studied properties of positive streamers at the ground pressure propagating in pure molecular nitrogen (N_2) gas and in 99% of N_2 with 1% admixture of molecular oxygen O_2 . The addition of O_2 led to enhancement of photoionization and resultant increase in levels of preionization ahead of the model streamers, which led to reductions in E_h/E_b and N_s and expansion of the streamer. Although the physical mechanism for changes in preionization levels considered by Pancheshnyi *et al.* [2001] is different from the quenching effects considered in this paper, the qualitative trends are essentially the same, reflecting effects of changes in levels of preionization on streamer properties.

[33] An analytical model allowing simple interpretation of the observed effects of preionization has been discussed in [Dyakonov and Kachorovskii, 1989; Babaeva and Naidis, 1997, and references therein]. The model considers effective residence time of electrons in the streamer head $\tau_h = r_s/(v_s \pm v_d(E_h))$ over which the electron density increases from N_{oe} ahead of the streamer to $N_s = N_{oe}e^{\nu_h \tau_h}$, where the plus and minus signs correspond to the positive and negative streamers respectively and ν_h is the value of the ionization coefficient at the field E_h (i.e., $\nu_h = \nu_i(E_h)$). Combining the expression $\nu_h \tau_h = \ln(N_s/N_{oe})$ with an equation describing equality of the conduction current in the streamer body and the displacement current in the streamer head, and an equation equalizing rates of the ionization and dielectric relaxation in the streamer head, leads to the following equation establishing a link between E_h/E_b and N_s/N_{oe} [Babaeva and Naidis, 1997]:

$$\frac{E_h}{E_b} \simeq \left[(1 \pm \zeta) \ln \left(\frac{N_s}{N_{oe}} \right) \right]^{1/\alpha} \quad (17)$$

where $\zeta = v_d(E_h)/v_s$ and $\alpha = 0.79$. We note that differences between positive and negative streamers are diminishing when $v_s \gg v_d(E_h)$ (i.e., $\zeta \gg 1$) [Babaeva and Naidis, 1997]. The substitution in this expression of numerical values N_s/N_{oe} discussed above and corresponding v_s and $v_d(E_h)$ values

listed in Table 2 leads to estimates $E_h/E_b = 16.7$ and 8.43 at altitudes 0 and 70 km, respectively, which agree well with previously discussed values 15.2 and 6.3 obtained from our numerical experiments. On simple physical grounds one would generally expect that a streamer would require a lower E_h field to bring its density to a given N_s value in cases when an enhanced preionization background is available ahead of it. For the purposes of the discussion, which will follow in section 4.4, we also note that a strong reduction of the preionization ahead of the streamer is expected to lead to a very high E_h/E_b ratios.

4.2. Similarity Laws for Streamers

[34] The results presented in Figure 4c and Tables 1 and 2 for models streamers at 70 km can be used to determine streamer properties at other altitudes of interest in sprite studies (40–90 km) using simple similarity scaling for time $\sim N$, length $\sim 1/N$ and streamer density $\sim N^2$ [Pasko *et al.*, 1998]. For example, a double-headed streamer initiated by a single electron avalanche at altitude of 80 km (note that $N(70 \text{ km})/N(80 \text{ km}) \simeq 4.52$) in applied field $1.5E_k$ ($E_k(80 \text{ km}) = 48.4 \text{ V/m}$) at the moment of time $181 \mu\text{s}$ would look exactly as the one shown in Figure 4c, if the simulation box dimensions $38 \text{ m} \times 210 \text{ m}$ are replaced with the scaled $172 \text{ m} \times 950 \text{ m}$ and the density scale is reduced by a factor of $4.52^2 = 20.43$. For the positive streamer at 80 km at time $181 \mu\text{s}$, $N_s = 3.46 \times 10^{10} \text{ m}^{-3}$, $N_{oe} = 2.42 \times 10^8 \text{ m}^{-3}$, $r_s = 29.4 \text{ m}$, $dv_s/dL = 1.17 \times 10^4$, with the rest of characteristics (E_h/E_k , E_b/E_k , v_s , $v_d(E_h)$, ΔU_h , dr_s/dL) being the same as listed in Table 2.

4.3. Acceleration and Expansion of Streamers

[35] The fast expansion and acceleration are important characteristics of the considered model streamers. For instance, a positive streamer initiated in $1.1E_k$ field at 70 km (see Table 3) would reach effective radius of 55 m and speed of about one tenth of the speed of light ($2.2 \times 10^7 \text{ m/s}$) by traveling a distance of only 1 km. Such high speeds of sprite streamers indeed have been recently documented by high-speed video [Stanley *et al.*, 1999; Moudry *et al.*, 2002, 2003] and multichannel photometric [McHarg *et al.*, 2002] systems. The initiation of sprites at altitudes 70–75 km in a form of simultaneous upward and downward propagating streamers is also well documented [Stanley *et al.*, 1999; Stenbaek-Nielsen *et al.*, 2000; Moudry *et al.*, 2002, 2003; McHarg *et al.*, 2002]. It is clear, however, that the effective streamer diameters observed by an imager zooming on a sprite structures at different altitudes would inevitably depend on the geometry of the mesospheric electric fields and the history of the sprite development (i.e., the altitude of the initiation point(s)). Gerken *et al.* [2000] and Gerken and Inan [2002, 2003] have recently employed a novel telescoping imager to measure effective streamer diameters at different altitudes in sprites. The measured diameters are 61–145, 150, 196 m, for altitude ranges 60–64, 76–80, 81–85 km, respectively. Although the 61–145 m is more than one order of magnitude greater than the scaled initial diameters of streamers shown in Figure 4c (at 60 km, $2r_s \simeq 4 \text{ m}$), given realistic charge moments available for the sprite initiation [Hu *et al.*, 2002], it is likely that streamers appearing at these low altitudes were initiated at much higher altitudes and propagated long

distances experiencing substantial expansion. All observed diameters by Gerken *et al.* [2000] and Gerken and Inan [2002, 2003] can therefore be realistically accounted for by the modeling studies presented in this paper.

[36] Simple estimates based on the measured charge moment changes in sprite producing lightning discharges [Hu *et al.*, 2002] show that large-scale electric fields exceeding E_k are easily available at mesospheric altitudes on vertical scales of many km. A question therefore arises about physical factors, which limit growth of the velocity and radius of the streamers in sprites as they propagate long distances. We emphasize that the model formulation presented in section 2 and used to produce results reported in section 3, does not prevent the streamer velocities from reaching and exceeding the speed of light.

[37] There are three principal factors, which would limit acceleration and expansion of streamers: (1) A reduction of the electric field in the streamer head because of the oppositely directed curl electric field generated by the changing magnetic field at the streamer front in accordance with the Faraday law of induction [Dyakonov and Kachorovskii, 1989]; (2) A collective action of multiple streamers on the applied electric field leading to self-consistent reduction of the field and growth rates of the streamers [e.g., Pasko *et al.*, 2000, 2001]; (3) A streamer branching, which is commonly observed in high-speed and telescopic video records of sprites [Stanley *et al.*, 1999; Moudry *et al.*, 2002, 2003; Gerken *et al.*, 2000; Gerken and Inan, 2002, 2003], and is also extensively documented in laboratory experiments with streamer coronas, as will be discussed in section 4.5.

[38] Dyakonov and Kachorovskii [1989] provide simple expressions allowing order of magnitude estimates for the maximum streamer radius r_{smax}^i and the streamer velocity v_{smax}^i , as limited by the induction effects. These equations can be easily derived from the Faraday law of induction and other equations discussed in section 4.1 linking various streamer characteristics, by setting the induction field equal to the streamer head field. Using the same notations as adopted earlier in our paper, these expressions are [Dyakonov and Kachorovskii, 1989]:

$$r_{\text{smax}}^i \sim \frac{c}{v_h} \left[\ln \left(\frac{N_s}{N_{oe}} \right) \right]^{\frac{1}{2}} \quad (18)$$

$$v_{\text{smax}}^i \sim c \left[\ln \left(\frac{N_s}{N_{oe}} \right) \right]^{-\frac{1}{2}} \quad (19)$$

where c is the speed of light in free space. Using numerical values of parameters provided in Table 2 for the positive streamer at 70 km altitude discussed in section 4.1, we obtain $r_{\text{smax}}^i \sim 114 \text{ m}$ and $v_{\text{smax}}^i \sim 0.45c$. However, as will be discussed in section 4.4, because of a fixed photoionization range in air, the expansion of a streamer is expected to lead to a reduction in N_{oe} (i.e., increase in $\ln(N_s/N_{oe})$ values), so that the actual radius at which induction effects become important is expected to be greater than 114 m and the streamer speed less than $0.45c$. One of the important conclusions, which follows from this consideration, is that streamer velocity always remains well below the speed of light.

[39] The ability of the streamer coronas to reduce macroscopic electric fields in the regions of space through

which they propagate is well documented and will not be discussed in detail here. The interested readers can find related references by *Pasko et al.* [2000, 2001]. We note, that the streamer branching is an essential component of the large-scale models of streamer coronas based on a fractal approach. However, this effect is introduced in these models on purely phenomenological grounds [e.g., *Pasko et al.*, 2000, 2001, and references therein]. In view of the importance of the streamer branching for understanding of the limitations on acceleration and expansion of streamers reported in this paper, the effect will be discussed in more detail in a separate section 4.4, which follows.

4.4. Branching of Streamers

[40] We note that finding exact physical factors, which define the transverse spatial scale of a streamer, is a difficult task since simplified streamer models do not usually provide a characteristic spatial scale for the streamer radius [e.g., *Raizer and Simakov*, 1998; *Bazelyan and Raizer*, 1998, p. 277; *Kulikovsky*, 2000, and references therein]. It has recently been demonstrated that negative streamers developing in high ambient fields, when no preionization available ahead of the streamer, are reaching an unstable “ideal conductivity” state with approximately equipotential and weakly curved head [*Arrayas et al.*, 2002; *Rocco et al.*, 2002]. It was proposed that this new state exhibits a Laplacian instability, like that in viscous fingering, which leads to branching of the streamer [*Arrayas et al.*, 2002; *Rocco et al.*, 2002].

[41] We have performed a set of simulation runs under conditions identical to those specified by *Arrayas et al.* [2002] (i.e., with no photoionization included) using the streamer model described in section 2 (i.e., based on modified Scharfetter-Gummel algorithm of [*Kulikovsky*, 1995]), as well as a model based on the second-order central fluxes with Zalesak flux correction [*Zalesak*, 1979], similar to that employed in [*Pasko et al.*, 1998]. Our results appeared to be identical to those reported by *Arrayas et al.* [2002], in terms of the specific details of the flattening of the streamer front and its time evolution toward the unstable state. We did observe the bifurcation of the streamer to a new state with a smaller transverse scale in our models, however, the specific morphology of the splitting was different in all three models we compared. Although, all models discussed are fully deterministic models and the streamer tip splitting results are expected to depend to some degree on the type of the numerical scheme employed (i.e., levels of numerical diffusion) [e.g., *Arrayas et al.*, 2002], the approach of the streamer to the unstable state was clearly demonstrated by all three models. We also noted that, (1) the unstable state very similar to the one reported by *Arrayas et al.* [2002] and *Rocco et al.* [2002] can be achieved at low applied electric fields, when the streamer transverse scale exceeds a certain threshold, as was demonstrated by *Pasko et al.* [1998] (Figure 4b); (2) the results are quite sensitive to the preionization ahead of the streamer, which generally acts to suppress the occurrence of the instability.

[42] In our present modeling, heads of both positive and negative streamers produce preionization through the photoionization effect. The electron energy requirements for the excitation of UV emitting states of N_2 are similar to those required for the ionization of O_2 [*Zheleznyak et al.*,

1982]. The relatively narrow region of peak electric field in the streamer head (see Figures 6a and 7a) therefore serves as a primary producer of the photoionizing UV photons, which generate electron-ion pairs ahead of the streamer. The ability of both positive and negative streamers to propagate without splitting should therefore depend on the ability of the photoionizing radiation to “escape” from the streamer head in order to produce the preionization ahead of the streamer. Considering schematics of the streamer head shown in Figure 2b, it is convenient to measure all distances appearing in the photoionization model given by equations (7), (14), and (15) in units of the streamer radius. One can interpret the streamer shown in the upper panel of Figure 2b as a result of evolution of the streamer shown in the lower panel after it expanded by a factor of five. Suppose that in both cases we want to estimate a number of photoionizing events per unit volume per unit time (i.e., dQ_{ph}/dV_2 given by equation (7)) at points A' and A at some specified distance from the streamer head (i.e., $r = 5r_s$ depicted in Figure 2b). We note that for both streamers the effective emission volume in equation (7), dV_1 , can be effectively approximated by the cube of the streamer head radius (i.e., $dV_1 \simeq r_s^3$). Substituting this expression in equation (7), assuming $r = 5r_s$ and using equations (14) and (15), it can be easily verified that the geometrical factors containing the streamer radius entering in the numerator and denominator of equation (7) compensate each other, except for the exponential terms coming from the function $g(r)$ (equation (15)). dQ_{ph}/dV_2 is proportional to $\exp(-\chi_{min}p_{O_2}5r_s)$, where we account for the fact that $\chi_{max}p_{O_2}r \gg 1$ for distances r on the order of or greater than the streamer radius r_s . It is clear from this consideration that at the same effective distance from the streamer head (e.g., $5r_s$) a “small” streamer with $r_s \ll 1/\chi_{min}p_{O_2}$ would generate more electron-ion pairs per unit volume per unit time than a “large” streamer with $r_s \gg 1/\chi_{min}p_{O_2}$ (i.e., $dQ_{ph}(A')/dV_2 \ll dQ_{ph}(A)/dV_2$ as shown in Figure 2b). The exponential factor ($-\chi_{min}p_{O_2}r$) entering in equation (15) of the photoionization model is therefore important for the characterization of the “escape” of UV photons from the streamer head and should be used for definition of the effective photoionization range of the streamer. It follows from this consideration that the effective photoionization range L_{ph} should be simply proportional to $1/\chi_{min}p_{O_2}$. This range, which does not change during the streamer expansion, is shown schematically in Figure 2b.

[43] Because of the fact that the photoionization range remains constant (for a given pressure), the preionization levels ahead of the streamer are reduced with the streamer expansion. As both negative and positive streamers expand, they would first try to compensate the reduction in preionization levels by increasing their E_h/E_b values as demonstrated by our results presented earlier in this paper, therefore moving closer to the unstable “ideal conductivity” state [*Arrayas et al.*, 2002; *Rocco et al.*, 2002]. The further expansion of the streamer and the reduction in preionization levels would lead to the saturation of the ionization coefficient at high E_h field and formation of approximately equipotential and weakly curved head, which would exhibit the splitting instability producing small-scale streamers, which are able to propagate with the small fixed photoionization range defined only by χ_{min} and p_{O_2} .

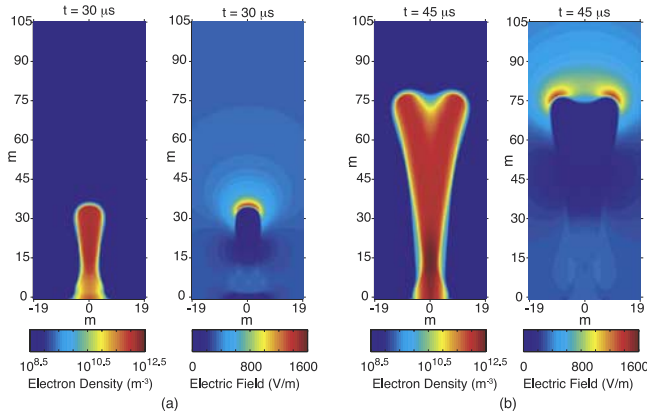


Figure 8. A cross-sectional view of the distribution of the electron number density and the electric field for a model positive streamer at 70 km altitude discussed in the text, right (a) before and (b) after the branching instability.

[44] No splitting of streamers was observed in our model under conditions of model runs specified in Figure 4. The extension of the simulation box sizes to follow dynamics of expanding streamers up to the branching point remains impossible at present because of prohibitively long model execution times. The above discussion about the photoionization range, however, indicates that the maximum radius of the streamer, after which the splitting should develop, can be expressed in a form $r_{\text{smax}} \simeq \kappa / \chi_{\text{min}} p_{\text{O}_2}$, where κ is a dimensionless parameter to be determined. This parameter is expected to be different for positive and negative streamers, and also for streamers at sprite altitudes and at the ground level reflecting changes in general photoionization levels due to the quenching effects discussed earlier in this paper. Although calculations are not possible at this time, one still can test the general concept by, (1) artificially changing the effective photoionization range by varying numerical values of χ_{min} and χ_{max} ; (2) keeping the photoionization range constant, but increasing the initial transverse size of the model streamers [e.g., Pasko *et al.*, 1998]; (3) increasing the magnitude of the applied electric field [Arrayas *et al.*, 2002; Rocco *et al.*, 2002].

[45] Figure 8 shows development of the positive streamer in electric field $1.5E_k$, which was initiated by a cloud of plasma placed at the anode, with characteristics similar to those employed for runs presented in Figure 4c (i.e., with Gaussian scale 3 m). The χ_{max} was set to a large value so that this parameter does not contribute to the photoionization levels ahead of the streamer (like in real case), and χ_{min} was varied by simple trial and error until the value $\chi_{\text{min}} = 0.9 \text{ cm}^{-1} \text{ Torr}^{-1}$ was found at which splitting was achieved approximately in the middle of the simulation domain, as shown in Figure 8. The approach to the unstable state, which we observed, was very similar to the previously reported results for negative streamers [Arrayas *et al.*, 2002; Rocco *et al.*, 2002] and in agreement with the arguments presented above. The radius of the streamer right before the onset of the splitting instability at time $\sim 30 \mu\text{s}$, is 3.8 m, so that an estimate for $\kappa_+ \simeq 3.5$ can be obtained in this case.

[46] We have not observed branching of negative streamers in our model in electric field $1.5E_k$ under initial

conditions similar to those which were used to produce results for positive streamers shown in Figure 8. The branching was not observed even in the case when no photoionization was included in the calculations (i.e., $\chi_{\text{min}} \rightarrow \infty$, $\chi_{\text{max}} \rightarrow \infty$). Figure 9 illustrates results obtained for a test case when $\chi_{\text{min}} = 0.9 \text{ cm}^{-1} \text{ Torr}^{-1}$, but the initial size of the streamer was increased by a factor of 5 and simulation box size by a factor of 2 in comparison with the positive streamer case. In this case the radius of the streamer right before the onset of the splitting instability at time 26 μs , is 15.2 m, which leads to an estimate $\kappa_- \simeq 14.1$.

[47] The above κ_{\pm} estimates can be used to obtain estimates for the maximum positive r_{smax}^+ and negative r_{smax}^- streamer radius at typical sprite altitudes. At 70 km, in particular, $r_{\text{smax}}^+ \simeq 97 \text{ m}$; $r_{\text{smax}}^- \simeq 390 \text{ m}$. It is important to emphasize that the splitting onset time observed in our experiments was quite sensitive to the spatial resolution of the model, and that increase in the resolution generally led to a delay in development of the instability, in agreement with results reported by Arrayas *et al.* [2002]. Therefore the numerical values κ_+ and κ_- and maximum streamer radii obtained above should only be considered as order of magnitude estimates, at best approximately valid at low air pressures corresponding to sprite altitudes. A separate analysis should be performed at high pressures (i.e., at the ground level), where we generally expect lower values of κ_+ and κ_- and smaller splitting diameters of streamers because of the quenching effects, which lead to the additional reduction in levels of photoionization ahead of streamers. Nevertheless, the results clearly demonstrate asymmetry between positive and negative streamers, indicating that positive streamers branch more often under otherwise identical ambient conditions, which is expected to be a common effect for streamers at high and low pressures. The upward (negative streamers) and downward (positive streamers) branching has been seen at least in some of the sprites [Moudry *et al.*, 2003; Gerken and Inan, 2003]. However, no detailed studies comparing the branching are presently available. Some types of sprites, called “carrot” sprites, do exhibit wider and less bifurcated upper branches and smaller scale and more bifurcated lower tendrils [Moudry *et al.*, 2003]. The comparison of these, however, is difficult

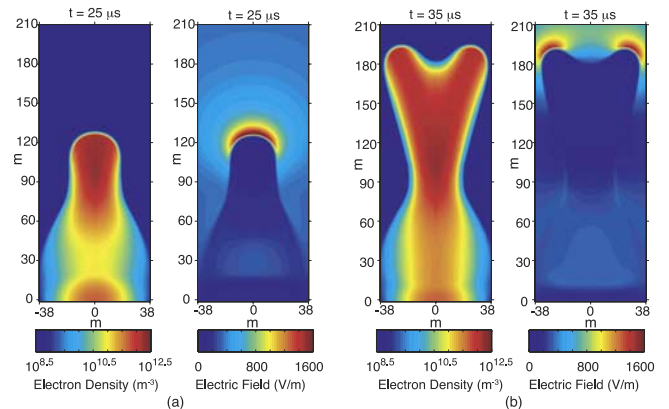


Figure 9. The same as Figure 8 only for a model negative streamer. Note a factor of 5 increase in the initial streamer radius and a factor of 2 increase in the simulation domain size in comparison with Figure 8.

because carrot sprites tend to extend many atmospheric-scale heights in altitude, so that pressure-dependent effects on streamer spatial scales due to the similarity laws $\sim 1/N$ [Pasko *et al.*, 1998] may interplay with the expansion of streamers because of their long propagation distances. Some related studies on branching of positive and negative streamers, performed in laboratory experiments, have recently become available and will be discussed in section 4.5.

[48] We note that importance of a photoionization range for the definition of the streamer radius has been recently discussed by Kulikovskiy [2000], who proposed an estimate $l_a \simeq 0.083$ mm for streamers in air at the ground pressure. We support the general idea advanced by Kulikovskiy [2000], but our reasoning for the definition of the photoionization range is different since we do not include the $1/r$ factor appearing in $g(r)$ given by equation (15) in this definition. We therefore obtain estimates of the streamer radius, which are two orders of magnitude greater than those estimated by Kulikovskiy [2000]. Interested readers are referred to [Pancheshnyi and Starikovskii, 2001; Kulikovskiy, 2001, 2002; Ebert and Hundsdorfer, 2002] for more discussion on related topics.

4.5. Comparison With Recent Laboratory Experiments

[49] The importance of the photoionization processes for the propagation of ionizing space charge waves in gases had been recognized many decades ago [e.g., Winn, 1967, and references cited therein]. In this section we provide a discussion of some recent experimental studies of laboratory streamers with unprecedented (ns and sub ns) time resolution, which emphasize the role of the photoionization effects on the streamer dynamics, and on the phenomenology of streamer branching, in particular.

[50] Yi and Williams [2002] have recently reported laboratory studies of positive and negative streamers in near atmospheric pressures N_2 and N_2/O_2 gas mixtures. The streamers were studied in $\simeq 13$ cm gap with voltage rise times around 20 ns and typical streamer initiation times 30–50 ns. We note that 13 cm and 20 ns scale to ~ 2 km and ~ 0.3 ms at 70 km, in accordance with the similarity laws discussed above, which are of the same order as the spatial scales of structures observed in sprites and the rise times associated with lightning quasi-static electric fields which drive the sprite phenomena. The streak camera provided ~ 2 ns resolution, which scales to 0.03 ms, a factor of three better than the 0.1 ms resolution achieved with multichannel photometers in sprite studies [McHarg *et al.*, 2002], while the shutter camera photos were taken with exposure times of 10 ns, which scales to 0.15 ms, an order of magnitude better than high-speed video resolution of 1 ms achieved in sprite studies [Stanley *et al.*, 1999; Stenbaek-Nielsen *et al.*, 2000; Moudry *et al.*, 2002, 2003] (referring to the 70 km altitude). The typical electric fields used in experiments of Yi and Williams [2002] were on the order of 10 kV/cm, which are a factor of four lower than those discussed in our paper. However, some experiments were conducted at low pressures with the same applied voltages so effective fields in excess of $1.6E_k$ were considered [Yi and Williams, 2002, Figure 10]. In this case streamers did exhibit propagation speeds exceeding 10^7 m/s in good agreement with overvolted streamers observed in sprites [Stanley *et al.*, 1999; Moudry *et al.*,

2002, 2003; McHarg *et al.*, 2002] and results on streamer acceleration presented in this paper. A more frequent branching of positive streamers in comparison with negative ones was noted in both N_2 and N_2/O_2 mixtures. Streamers branched more frequently in N_2 and addition of small amounts of O_2 sharply reduced the branching. The addition of O_2 also increased the streamer propagation speed. All these effects were attributed by the authors to increase in the photoionization range, which is considerably longer for O_2 than N_2 [Yi and Williams, 2002]. These findings generally support the theoretical arguments discussed in this paper. In N_2 with 10% O_2 the measured diameters of positive (6 mm) and negative (8 mm) streamers are in good agreement with scaled diameters observed in sprites [Gerken *et al.*, 2000; Gerken and Inan, 2002, 2003] (6 and 8 mm scale to ~ 90 and 120 m, respectively, at 70 km altitude).

[51] van Veldhuizen and Rutgers [2002] have reported studies of positive streamers in air in 2.5 cm gap with voltages up to 25 kV and voltage rise times less than 25 ns. Unique photographs of streamers with time exposures of only 0.8 ns were obtained. The work emphasized studies of streamer branching. The results indicate significant dependence of branching on electrode geometry, in particular, a factor of 10 increase in branching in a point wire gap in comparison with a plane protrusion gap. Also, it was established that enhanced branching in air occurs if a resistance is included in the pulse circuit [van Veldhuizen *et al.*, 2002; van Veldhuizen and Rutgers, 2002]. These findings indicate that branching is a complex phenomenon, which in real systems depends on a number of factors, in addition to the photoionization range and the electric field magnitude discussed in our paper. The authors noted a very high sensitivity of the speed of propagation of streamers in response to the applied voltage increases. These results qualitatively agree with our findings presented in Table 3, indicating ~ 2.5 times increase in v_s and dv_s/dL in response to $\sim 35\%$ increase in the applied electric field.

5. Conclusions

[52] The principal results and contributions, which follow from studies presented in this paper, can be summarized as follows:

[53] 1. Development of a new two-dimensional streamer model with the inclusion of N_2 singlet state photoemission and subsequent O_2 photoionization processes, which allows studies of double-headed streamers and associated time resolved optical emissions and photoionization effects in air for a wide range of air pressures.

[54] 2. Identification of the quenching of the excited $b^1\Pi_u$, $b'^1\Sigma_u^+$ and $c_4'^1\Sigma_u^+$ singlet states of N_2 , which are responsible for the photoionization in air, as a physical process, which is responsible for nonsimilar behavior of streamers at different pressures, leading in particular, to lower peak electric fields in the streamer head, lower streamer electron densities, wider initial streamer structures, and lower acceleration and expansion rates of streamers at sprite altitudes 40–90 km, when compared to the ground level.

[55] 3. Documentation of rates of expansion and acceleration of streamers in air in a homogeneous applied electric field for a range of field magnitudes and air pressures,

which provides quantitative explanation of the propagation speeds and spatial scales of streamers obtained during recent telescopic, high-speed video and multicannel photometric observations of sprites.

[56] 4. Identification of the absorption cross section of O₂ at 1025 Å as a principal parameter, which defines the pressure-dependent photoionization range in air and branching scales of streamers.

[57] **Acknowledgments.** This research was supported by NASA NAG5-11832 and NSF ATM-0134838 grants to Penn State University. We gratefully acknowledge assistance of Tom Heffner in development of software for the optical emission model. We wish to thank Ute Ebert, Eddie van Veldhuizen, Wijnand Rutgers and Willem Hundsdorfer for useful discussions. We also thank two reviewers for many useful comments and suggestions.

[58] Arthur Richmond thanks Russell Armstrong and David Sentman for their assistance in evaluating this manuscript.

References

- Armstrong, R. A., J. A. Shorter, M. J. Taylor, D. M. Suszcynsky, W. A. Lyons, and L. S. Jeong (1998), Photometric measurements in the SPRITES' 95 and 96 campaigns of nitrogen second positive (399.8 nm) and first negative (427.8 nm) emission, *J. Atmos. Solar Terr. Phys.*, **60**, 787–799.
- Armstrong, R. A., D. M. Suszcynsky, W. A. Lyons, and T. E. Nelson (2000), Multi-color photometric measurements of ionization and energies in sprites, *Geophys. Res. Lett.*, **27**, 653–657.
- Arrayas, M., U. Ebert, and W. Hundsdorfer (2002), Spontaneous branching of anode-directed streamers between planar electrodes, *Phys. Rev. Lett.*, **88**, 174502(R), doi:10.1103/PhysRevLett.88.174502.
- Babaeva, N. Y., and G. V. Naidis (1996), Two-dimensional modeling of positive streamer dynamics in non-uniform electric fields in air, *J. Phys. D Appl. Phys.*, **29**, 2423–2431.
- Babaeva, N. Y., and G. V. Naidis (1997), Dynamics of positive and negative streamers in air in weak uniform electric fields, *IEEE Trans. Plasma Sci.*, **25**, 375–379.
- Babaeva, N. Y., and G. V. Naidis (2001), On streamer dynamics in dense media, *J. Electrostat.*, **53**, 123–133.
- Barrington-Leigh, C. P. (2000), Fast photometric imaging of high altitude optical flashes above thunderstorms, Ph.D. thesis, Stanford Univ., Stanford, Calif.
- Barrington-Leigh, C. P., V. P. Pasko, and U. S. Inan (2002), Exponential relaxation of optical emissions in sprites, *J. Geophys. Res.*, **107**(A5), 1065, doi:10.1029/2001JA900117.
- Bazelyan, E. M., and Y. P. Raizer (1998), *Spark Discharge*, Chem. Rubber Co., New York.
- Bucselo, E., J. Morrill, M. Heavner, C. Siefring, S. Berg, D. Hampton, D. Moudry, E. Wescott, and D. Sentman (2003), N₂ (B³Π_g) and N₂⁺ (A²Π_u) vibrational distributions observed in sprites, *J. Atmos. Solar Terr. Phys.*, **65**, 583–590.
- Carter, V. L. (1972), High resolution N₂ absorption study from 730 to 980 Å, *J. Chem. Phys.*, **56**, 4195–4205.
- Chamberlain, J. W. (1978), *Theory of Planetary Atmospheres*, Academic, San Diego, Calif.
- Davies, D. K. (1983), Measurements of swarm parameters in dry air, in *Theoretical Notes*, Note 346, Westinghouse R&D Cent., Pittsburgh, Pa.
- Dehmer, P. M., and W. A. Chupka (1975), High resolution study of photoionization processes in O₂, *J. Chem. Phys.*, **62**, 4525–4534.
- Dhali, S. K., and P. F. Williams (1987), Two-dimensional studies of streamers in gases, *J. Appl. Phys.*, **62**, 4696–4707.
- Dutton, J. (1975), A survey of electron swarm data, *J. Phys. Chem. Ref. Data*, **4**, 577–856.
- Dyakonov, M. I., and V. Y. Kachorovskii (1989), Streamer discharge in a homogeneous field, *Sov. Phys. JETP, Engl. Transl.*, **68**, 1070–1074.
- Ebert, U., and W. Hundsdorfer (2002), Comment on “Spontaneous branching of anode-directed streamers between planar electrodes”—Reply, *Phys. Rev. Lett.*, **89**(22), doi:10.1103/PhysRevLett.89.229402.
- Gallagher, J. W., E. C. Beatty, J. Dutton, and L. C. Pitchford (1983), An annotated compilation and appraisal of electron swarm data in electro-negative gases, *J. Phys. Chem. Ref. Data*, **12**, 109–152.
- Gerken, E. A., and U. S. Inan (2002), A survey of streamer and diffuse glow dynamics observed in sprites using telescopic imagery, *J. Geophys. Res.*, **107**(A11), 1344, doi:10.1029/2002JA009248.
- Gerken, E. A., and U. S. Inan (2003), Observations of decameter-scale morphologies in sprites, *J. Atmos. Solar Terr. Phys.*, **65**, 567–572, doi:10.1016/S1364-6826(02)00333-4.
- Gerken, E. A., U. S. Inan, and C. P. Barrington-Leigh (2000), Telescopic imaging of sprites, *Geophys. Res. Lett.*, **27**, 2637–2640.
- Guo, J. M., and C. H. Wu (1993), Comparisons of multidimensional fluid models for streamers, in *Non-thermal Plasma Techniques for Pollution Control*, NATO ASI Ser., Ser. G, vol. 34(A), pp. 287–298, Springer-Verlag, New York.
- Hampton, D. L., M. J. Heavner, E. M. Wescott, and D. D. Sentman (1996), Optical spectral characteristics of sprites, *Geophys. Res. Lett.*, **23**, 89–93.
- Hockney, R. W., and J. W. Eastwood (1988), *Computer Simulation Using Particles*, McGraw-Hill, New York.
- Hu, W. Y., S. A. Cummer, and W. A. Lyons (2002), Lightning charge moment changes for the initiation of sprites, *Geophys. Res. Lett.*, **29**(8), 1279, doi:10.1029/2001GL014593.
- Kanik, I., L. W. Beegle, J. M. Ajello, and S. C. Solomon (2000), Electron-impact excitation/emission and photoabsorption cross sections important in the terrestrial airglow and auroral analysis of rocket and satellite observations, *Phys. Chem. Earth, Part C*, **25**, 573–581.
- Kossyi, I. A., A. Y. Kostinsky, A. A. Matveyev, and V. P. Silakov (1992), Kinetic scheme of the non-equilibrium discharge in nitrogen-oxygen mixtures, *Plasma Sources Sci. Technol.*, **1**, 207–220.
- Kulikovskiy, A. A. (1995), A more accurate Scharfetter-Gummel algorithm of electron transport for semiconductor and gas discharge simulation, *Comput. Phys.*, **119**, 149–155.
- Kulikovskiy, A. A. (1997a), Production of chemically active species in the air by a single positive streamer in a nonuniform field, *IEEE Trans. Plasma Sci.*, **25**, 439–446.
- Kulikovskiy, A. A. (1997b), The mechanism of positive streamer acceleration and expansion in air in a strong external field, *J. Phys. D Appl. Phys.*, **30**, 1515–1522.
- Kulikovskiy, A. A. (2000), The role of photoionization in positive streamer dynamics, *J. Phys. D Appl. Phys.*, **33**, 1514–1524.
- Kulikovskiy, A. A. (2001), Reply to comment on “The role of photoionization in positive streamer dynamics,” *J. Phys. D Appl. Phys.*, **34**, 251–252.
- Kulikovskiy, A. A. (2002), Comment on “Spontaneous branching of anode-directed streamers between planar electrodes,” *Phys. Rev. Lett.*, **89**(22), doi:10.1103/PhysRevLett.89.229401.
- Kunhardt, E. E., and Y. Tzeng (1988), Development of an electron avalanche and its transition into streamers, *Phys. Rev. A*, **38**, 1410–1421.
- Loeb, L. B., and J. M. Meek (1940), The mechanism of spark discharge in air at atmospheric pressure, *J. Appl. Phys.*, **11**, 438–447.
- Lofthus, A., and P. H. Krupenie (1977), The spectrum of molecular nitrogen, *J. Phys. Chem. Ref. Data*, **6**, 113–307.
- Lowke, J. J. (1992), Theory of electrical breakdown in air—The role of metastable oxygen molecules, *J. Phys. D Appl. Phys.*, **25**, 202–210.
- McHarg, M. G., R. K. Haaland, D. R. Moudry, and H. C. Stenbaek-Nielsen (2002), Altitude-time development of sprites, *J. Geophys. Res.*, **107**(A11), 1364, doi:10.1029/2001JA000283.
- Mende, S. B., R. L. Rairden, G. R. Swenson, and W. A. Lyons (1995), Sprite spectra: N₂ 1 PG band identification, *Geophys. Res. Lett.*, **22**, 2633–2637.
- Mnatsakanyan, A. K., and G. V. Naidis (1991), Charged particle production and loss processes in nitrogen-oxygen plasmas, in *Reviews of Plasma Chemistry*, vol. 1, edited by B. M. Smirnov pp. 259–292, Consult. Bur., New York.
- Morrill, J. S., E. J. Bucselo, V. P. Pasko, S. L. Berg, W. M. Benesch, E. M. Wescott, and M. J. Heavner (1998), Time resolved N₂ triplet state vibrational populations and emissions associated with red sprites, *J. Atmos. Solar Terr. Phys.*, **60**, 811–829.
- Morrill, J., et al. (2002), Electron energy and electric field estimates in sprites derived from ionized and neutral N₂ emissions, *Geophys. Res. Lett.*, **29**(10), doi:10.1029/2001GL014018.
- Morrow, R., and J. J. Lowke (1997), Streamer propagation in air, *J. Phys. D Appl. Phys.*, **30**, 614–627.
- Moudry, D. R., H. C. Stenbaek-Nielsen, D. D. Sentman, and E. M. Wescott (2002), Velocities of sprite tendrils, *Geophys. Res. Lett.*, **29**(20), 1992, doi:10.1029/2002GL015682.
- Moudry, D. R., H. C. Stenbaek-Nielsen, D. D. Sentman, and E. M. Wescott (2003), Imaging of elves, halos and sprite initiation at 1 ms time resolution, *J. Atmos. Solar Terr. Phys.*, **65**, 509–518, doi:10.1016/S1364-6826(02)00323-1.
- Naidis, G. V. (1997), Effects of nonlocality on the dynamics of streamers in positive corona discharges, *Tech. Phys. Lett.*, **23**, 493–494.
- Naidis, G. V. (1999), Simulation of streamer-to-spark transition in short non-uniform air gaps, *J. Phys. D Appl. Phys.*, **32**, 2649–2654.
- Pancheshnyi, S. V., and A. Y. Starikovskii (2001), Comments on “The role of photoionization in positive streamer dynamics,” *J. Phys. D Appl. Phys.*, **34**, 248–250.
- Pancheshnyi, S. V., S. M. Starikovskaia, and A. Y. Starikovskii (2001), Role of photoionization processes in propagation of cathode-directed streamer, *J. Phys. D Appl. Phys.*, **34**, 105–115.

- Pasko, V. P., and J. J. George (2002), Three-dimensional modeling of blue jets and blue starters, *J. Geophys. Res.*, *107*(A12), 1458, doi:10.1029/2002JA009473.
- Pasko, V. P., and H. C. Stenbaek-Nielsen (2002), Diffuse and streamer regions of sprites, *Geophys. Res. Lett.*, *29*(A10), doi:10.1029/2001GL014241.
- Pasko, V. P., U. S. Inan, T. F. Bell, and Y. N. Taranenko (1997), Sprites produced by quasi-electrostatic heating and ionization in the lower ionosphere, *J. Geophys. Res.*, *102*, 4529–4561.
- Pasko, V. P., U. S. Inan, and T. F. Bell (1998), Spatial structure of sprites, *Geophys. Res. Lett.*, *25*, 2123–2126.
- Pasko, V. P., U. S. Inan, and T. F. Bell (1999), Thermal runaway electrons in sprites, paper presented at 1999 URSI National Radio Science Meeting, Union Radio Sci. Int., Boulder, Colo.
- Pasko, V. P., U. S. Inan, and T. F. Bell (2000), Fractal structure of sprites, *Geophys. Res. Lett.*, *27*, 497–500.
- Pasko, V. P., U. S. Inan, and T. F. Bell (2001), Mesosphere-troposphere coupling due to sprites, *Geophys. Res. Lett.*, *28*, 3821–3824.
- Petrov, N. I., and G. N. Petrova (1999), Physical mechanisms for the development of lightning discharges between a thundercloud and the ionosphere, *Tech. Phys.*, *44*, 472–475.
- Raizer, Y. P. (1991), *Gas Discharge Physics*, Springer-Verlag, New York.
- Raizer, Y. P., and A. N. Simakov (1998), Main factors determining the radius of the head of a long streamer and the maximum electric field near the head, *Plasma Phys. Rep.*, *24*, 700–706.
- Raizer, Y. P., G. M. Milikh, M. N. Shneider, and S. V. Novakovski (1998), Long streamers in the upper atmosphere above thundercloud, *J. Phys. D Appl. Phys.*, *31*, 3255–3264.
- Rocco, A., U. Ebert, and W. Hundsdorfer (2002), Branching of negative streamers in free flight, *Phys. Rev. E*, *66*, 035102(R), doi:10.1103/PhysRevE.66.035102.
- Scharfetter, D. L., and H. K. Gummel (1969), Large-signal analysis of a silicon read diode oscillator, *IEEE Trans. Electr. Devices*, *16*, 64–77.
- Sentman, D. D., E. M. Wescott, D. L. Osborne, D. L. Hampton, and M. J. Heavner (1995), Preliminary results from the Sprites94 campaign: Red sprites, *Geophys. Res. Lett.*, *22*, 1205–1208.
- Sipler, D. P., and M. A. Biondi (1972), Measurements of O (¹D) quenching rates in the F region, *J. Geophys. Res.*, *77*, 6202–6212.
- Stanley, M., P. Krehbiel, M. Brook, C. Moore, W. Rison, and B. Abrahams (1999), High speed video of initial sprite development, *Geophys. Res. Lett.*, *26*, 3201–3204.
- Stenbaek-Nielsen, H. C., D. R. Moudry, E. M. Wescott, D. D. Sentman, and F. T. Sao Sabbas (2000), Sprites and possible mesospheric effects, *Geophys. Res. Lett.*, *27*, 3827–3832.
- Suszcynsky, D. M., R. Roussel-Dupre, W. A. Lyons, and R. A. Armstrong (1998), Blue-light imagery and photometry of sprites, *J. Atmos. Solar Terr. Phys.*, *60*, 801–809.
- Takahashi, Y., M. Fujito, Y. Watanabe, H. Fukunishi, and W. A. Lyons (2000), Temporal and spatial variations in the intensity ratio of N-2 1st and 2nd positive bands in SPRITES, *Adv. Space Res.*, *26*, 1205–1208.
- Vallance Jones, A. V. (1974), *Aurora*, D. Reidel, Norwell, Mass.
- van Veldhuizen, E. M. (ed.) (2002), *Electrical Discharges for Environmental Purposes: Fundamentals and Applications*, Nova Sci., New York.
- van Veldhuizen, E. M., and W. R. Rutgers (2002), Pulsed positive corona streamer propagation and branching, *J. Phys. D Appl. Phys.*, *35*, 2169–2179.
- van Veldhuizen, E. M., P. C. M. Kemps, and W. R. Rutgers (2002), Streamer branching in a short gap: The influence of the power supply, *IEEE Trans. Plasma Sci.*, *30*, 162–163.
- Vitello, P. A., B. M. Penetrante, and J. N. Bardsley (1993), Multidimensional modeling of the dynamic morphology of streamer coronas, in *Non-thermal Plasma Techniques for Pollution Control, NATO ASI Ser., Ser. G*, vol. 34(A), pp. 249–271, Springer-Verlag, New York.
- Vitello, P. A., B. M. Penetrante, and J. N. Bardsley (1994), Simulation of negative-streamer dynamics in nitrogen, *Phys. Rev. E*, *49*, 5574–5598.
- Walter, C. W., P. C. Cosby, and H. Helm (1994), Predissociation quantum yields of singlet nitrogen, *Phys. Rev. A*, *50*, 2930–2936.
- Wescott, E. M., D. Sentman, D. Osborne, D. Hampton, and M. Heavner (1995), Preliminary results from the Sprites94 aircraft campaign: 2. Blue jets, *Geophys. Res. Lett.*, *22*, 1209–1212.
- Wescott, E. M., D. D. Sentman, M. J. Heavner, D. L. Hampton, and O. H. Vaughan Jr. (1998), Blue jets: Their relationship to lightning and very large hailfall, and their physical mechanisms for their production, *J. Atmos. Solar Terr. Phys.*, *60*, 713–724.
- Winn, W. P. (1967), Ionizing space-charge waves in gases, *J. Appl. Phys.*, *38*, 783–790.
- Yi, W. J., and P. F. Williams (2002), Experimental study of streamer in pure N₂ and N₂/O₂ mixtures and a ≈13 cm gap, *J. Phys. D Appl. Phys.*, *35*, 205–218.
- Zalesak, S. T. (1979), Fully multidimensional flux-corrected transport algorithms for fluids, *J. Comput. Phys.*, *31*, 335–362.
- Zhao, X. M., J. C. Diels, C. Y. Wang, and J. M. Elizondo (1995), Femto-second ultraviolet laser pulse induced lightning discharge in gases, *IEEE J. Quantum Electr.*, *31*, 599–612.
- Zheleznyak, M. B., A. K. Mnatsakanyan, and S. V. Sizykh (1982), Photoionization of nitrogen and oxygen mixtures by radiation from a gas discharge, *High Temp.*, *20*, 357–362.

N. Liu and V. P. Pasko, Communications and Space Sciences Laboratory, Department of Electrical Engineering, Pennsylvania State University, University Park, PA 16802, USA. (nul105@psu.edu; vpasko@psu.edu)

Correction to “Effects of photoionization on propagation and branching of positive and negative streamers in sprites”

Ningyu Liu and Victor P. Pasko

Received 18 July 2004; published 15 September 2004.

INDEX TERMS: 2427 Ionosphere: Ionosphere/atmosphere interactions (0335); 3304 Meteorology and Atmospheric Dynamics: Atmospheric electricity; 3324 Meteorology and Atmospheric Dynamics: Lightning; 0310 Atmospheric Composition and Structure: Airglow and aurora; 2435 Ionosphere: Ionospheric disturbances; 9900 Corrections; **KEYWORDS:** corona streamers, photoionization, sprites

Citation: Liu, N., and V. P. Pasko (2004), Correction to “Effects of photoionization on propagation and branching of positive and negative streamers in sprites,” *J. Geophys. Res.*, *109*, A09306, doi:10.1029/2004JA010692.

[1] In the paper “Effects of photoionization on propagation and branching of positive and negative streamers in sprites” by Ningyu Liu and Victor P. Pasko (*Journal of Geophysical Research*, *109*, A04301, doi:10.1029/2003JA010064, 2004) some of the scalings of streamer characteristics as a function of air density N are incorrect. The correct text appears below.

[2] Paragraph [23]: In accordance with the similarity laws the streamer timescales, the streamer spatial scales, and the streamer electron densities scale with the air density as $\sim 1/N$ (not N as in the original manuscript), $\sim 1/N$, and $\sim N^2$, respectively, and the scaled streamer characteristics remain otherwise identical for the same values of the reduced electric field E/N [Pasko *et al.*, 1998].

[3] Paragraph [24]: The horizontal and vertical dimensions of the simulation boxes in Figures 4b and 4c also directly correspond to scaled ($\sim 1/N$ (not N as in the original manuscript)) ground values shown in Figure 4a.

[4] Paragraph [34]: The results presented in Figure 4c and Tables 1 and 2 for models streamers at 70 km can be used to determine streamer properties at other altitudes of interest in sprite studies (40–90 km) using simple similarity scaling for time $\sim 1/N$ (not N as in the original manuscript), length $\sim 1/N$, and streamer density $\sim N^2$ [Pasko *et al.*, 1998].

N. Liu and V. P. Pasko, CSSL Laboratory, Department of Electrical Engineering, Pennsylvania State University, University Park, PA 16802, USA. (nll105@psu.edu; vpasko@psu.edu)